Research Paper

Geosphere, published online on 5 February 2016 as doi:10.1130/GES01254.1

GEOSPHERE

GEOSPHERE; v. 12, no. 2

doi:10.1130/GES01254.1

12 figures; 3 tables; 1 supplemental file

CORRESPONDENCE: avz5818@gmail.com; azuza@ucla.edu

CITATION: Zuza, A.V., Cheng, X., and Yin, A., 2016, Testing models of Tibetan Plateau formation with Cenozoic shortening estimates across the Qilian Shan–Nan Shan thrust belt: Geosphere, v. 12, no. 2, doi:10.1130/GES01254.1.

Received 24 August 2015
Revision received 6 November 2015
Accepted 13 January 2016

THE GEOLOGICAL SOCIETY OF AMERICA®

For permission to copy, contact Copyright Permissions, GSA, or editing@geosociety.org.

© 2016 Geological Society of America

Testing models of Tibetan Plateau formation with Cenozoic shortening estimates across the Qilian Shan–Nan Shan thrust belt

Andrew V. Zuza[1], Xiaogan Cheng[2,3], and An Yin[1,4]

[1]Department of Earth, Planetary, and Space Sciences, University of California, Los Angeles, California 90095-1567, USA
[2]Department of Earth Sciences, Zhejiang University, Hangzhou 310027, China
[3]Research Center for Structures in Oil and Gas Bearing Basin, Ministry of Education, Hangzhou 310027, China
[4]Structural Geology Group, China University of Geosciences (Beijing), Beijing 10085, China

ABSTRACT

Competing models that account for the construction of the Tibetan Plateau include continental subduction, underthrusting, distributed shortening, channel flow, and older crustal-structure inheritance. Well-constrained estimates of crustal shortening strain serve as a diagnostic test of these plateau formation models and are critical to elucidate the dominant mechanism of plateau development. In this work we estimate the magnitude of Cenozoic shortening across the northern Qilian Shan–Nan Shan thrust belt, along the northeastern plateau margin, based on detailed analysis and reconstruction of three high-resolution seismic reflection profiles. By integrating surface geology, seismic data, and the regional tectonic history, we demonstrate that this thrust system has accumulated >53% Cenozoic strain (~50 km shortening), accommodated by several south-dipping thrust faults. Based on the observed strain distribution across northern Tibet, including lower strain (30%–45%) within the interior of the Qilian Shan–Nan Shan thrust belt, we suggest that a combination of distributed crustal shortening and minor (<250 km) southward underthrusting of the Asian lithosphere is responsible the development of the northern Tibetan Plateau. Focused shortening along the Qilian Shan frontal thrust system accommodates much of the present-day convergence between Tibet and North China, which implies that the northern plateau margin may have developed in a similar manner to that of southern Tibet through Himalayan-style continental underthrusting. We also argue that the Qilian Shan–Nan Shan, North Qaidam, and Qaidam Basin thrust systems have absorbed a minimum of 250–350 km north-south Cenozoic shortening, which is double the commonly cited value of ~150 km.

INTRODUCTION

Understanding how the Tibetan Plateau (Fig. 1) was constructed greatly affects our knowledge of continental tectonics (Molnar, 1988; Yin, 2010). End-member models for plateau formation and evolution include (Table 1) (1) Cenozoic distributed shortening of the Asian crust (Dewey and Bird, 1970; Dewey and Burke, 1973) or its entire lithosphere (England and Houseman, 1986), (2) Cenozoic underthrusting of Indian (Argand, 1924; Powell and Conaghan, 1973; Powell, 1986; DeCelles et al., 2002; van Hinsbergen et al., 2011, 2012) and/or Asian lithosphere (Willett and Beaumont, 1994; Kind et al., 2002; Zhao et al., 2011; Feng et al., 2014; Ye et al., 2015) beneath the Tibetan Plateau, (3) Cenozoic vertical inflation of Tibetan crust by lateral channel flow in the middle or lower crust (Zhao and Morgan, 1987; Bird, 1991; Royden et al., 1997, 2008; Clark and Royden, 2000), (4) discrete Cenozoic intracontinental subduction coupled with lateral extrusion along major strike-slip faults (Tapponnier et al., 2001), and (5) pre-Cenozoic crustal thickening (e.g., Worley and Wilson, 1996; Murphy et al., 1997; Wallis et al., 2003). These models make specific predictions regarding the spatial distribution, magnitude, and temporal variation of Cenozoic strain (Table 1; Fig. 2).

Estimates of shortening magnitude provide a quantitative and diagnostic test for differentiating between these tectonic models, especially along the plateau margins where the effects predicted by intracontinental subduction, underthrusting, and crustal inflation models are most pronounced (e.g., Clark and Royden, 2000; DeCelles et al., 2002; Hubbard and Shaw, 2009; Lease et al., 2012). For example, the predictions of the lower crustal flow model of Clark and Royden (2000) were initially supported by early observations of minimal east-west horizontal crustal shortening across the Longmen Shan along the eastern margin of the plateau (Fig. 1B) (Burchfiel et al., 1995; King et al., 1997). More recent seismic reflection analysis and balanced cross-section restoration indicate that crustal shortening alone is significant enough to generate the elevation and crustal thickness of the eastern Tibetan Plateau (Hubbard and Shaw, 2009). In the Laji Shan–West Qinling of northeastern Tibet (Fig. 1B), the present-day crustal thickness (45–55 km) (Yue et al., 2012) can be reconciled with crustal shortening strain of 10%–12% and pure shear crustal thickening (Lease et al., 2012).

Although investigations of Cenozoic shortening along the southern and eastern margins of the plateau have been robust (e.g., Burchfiel et al., 1995; Johnson, 2002; DeCelles et al., 2002; Robinson et al., 2006; McQuarrie et al., 2008; Hubbard and Shaw, 2009; Webb et al., 2011; Webb, 2013), our understanding of Cenozoic deformation along the northern plateau margin is lacking.

Geosphere, published online on 5 February 2016 as doi:10.1130/GES01254.1

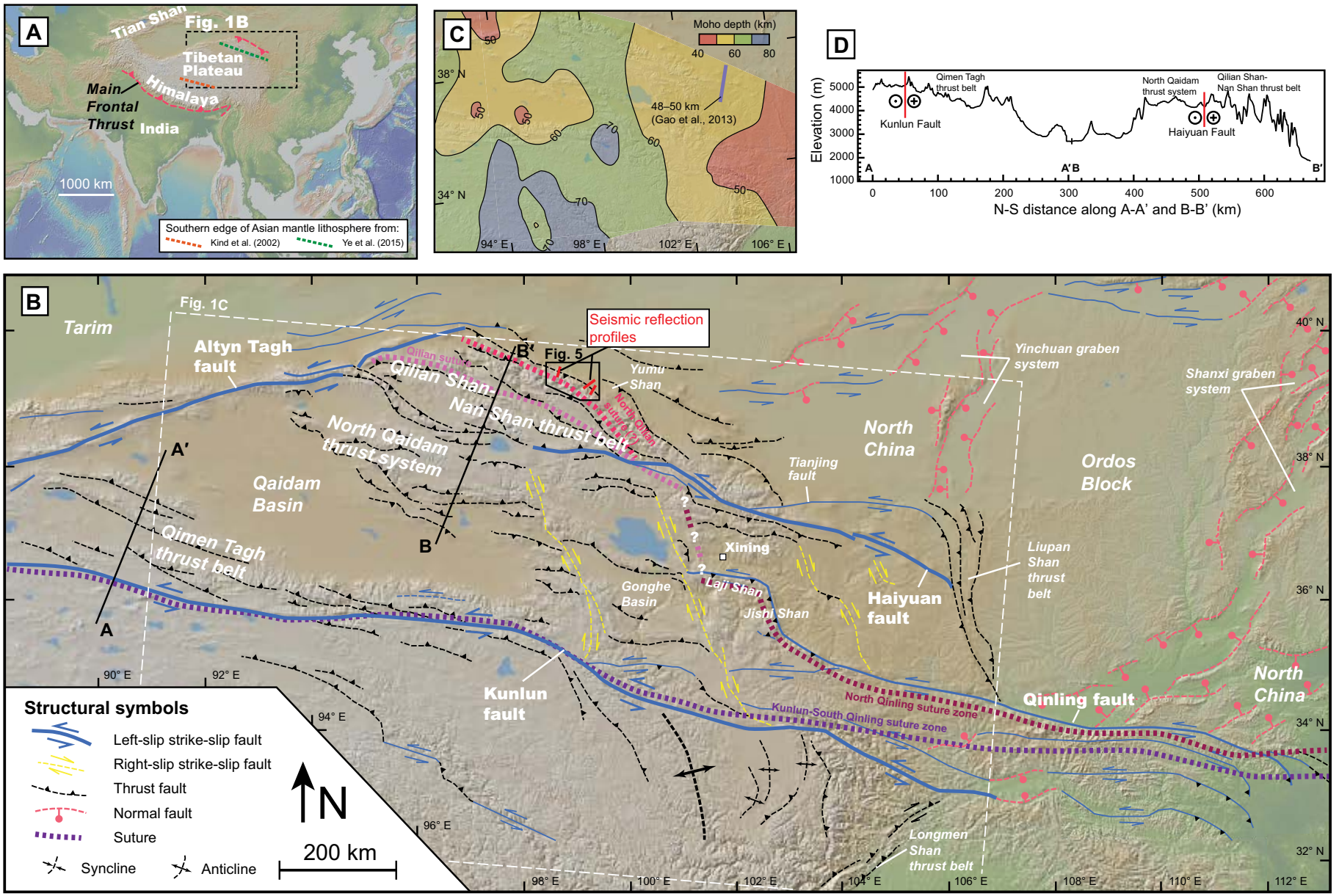

Figure 1. (A) Map of the Himalaya-Tibetan orogen and surrounding regions, showing the location of Figure 1B. The southern edge of Asian lithosphere is from Kind et al. (2002) and Ye et al. (2015). (B) Cenozoic fault map of the northeastern Tibetan Plateau showing the location of the detailed geologic map (Fig. 5), the seismic reflection profiles (Figs. 7–9), and location of C. Structures are from Burchfiel et al. (1991), Gaudemer et al. (1995), Taylor and Yin (2009), and Gao et al. (2013). (C) Contoured crustal thickness estimates derived from receiver-function analysis of Yue et al. (2012). Also shown for comparison is the Moho depth imaged by seismic reflection analysis of Gao et al. (2013). (D) Topographic profiles across northeastern Tibet (profiles A–A' and B–B' in B). The digital topographic basemaps and profiles from GeoMapApp software (Ryan et al., 2009) are available at http://www.geomapapp.org/.

Geosphere, published online on 5 February 2016 as doi:10.1130/GES01254.1

TABLE 1. COMPARISON OF MODEL PREDICTIONS FOR THE FORMATION OF THE TIBETAN PLATEAU

	Predictions			
Models	Temporal evolution	Spatial distribution	Shortening at plateau margins	References
Distributed shortening	Northward propagation of shortening across Tibet	Cenozoic thrusts and folds are uniformly distributed across Tibet	30%–40% crustal shortening to explain the crustal thickness of Tibet	Dewey and Bird (1970); Dewey and Burke (1973); England and Houseman (1986)
Discrete intracontinental subduction	Stepwise, northward propagation of the intracontinental subduction zones	Cenozoic thrusts in discrete zones along older sutures and coeval strike-slip faults	Little shortening away but >50% shortening along the subduction zones	Meyer et al. (1998); Tapponnier et al. (2001)
Underthrusting of Indian and/or Asian lithosphere	Shortening propagates inward from underthrust margins (e.g., north from Himalaya and south from Qilian Shan)	Cenozoic structures contributing to crustal thickening are minor features in Tibet	>50% crustal shortening along plateau margins but little shortening within plateau	Argand (1924); Powell and Conaghan (1973); Powell (1986); Kind et al. (2002); Zhao et al. (2011); Ye et al. (2015)
Vertical inflation by channel flow	Propagating surface uplift from plateau interior to plateau margins	Minor Cenozoic shortening particularly along plateau margins	Little crustal shortening (<5%), particularly along plateau margins	Zhao and Morgan (1987); Bird (1991); Royden et al. (1997); Clark and Royden (2000); Karplus et al. (2011)
Inherited thickness	Deformation and structures predate India-Eurasian collision	Structures related to pre-Cenozoic tectonic settings	Mainly pre-Cenozoic structures and minimal erosion	Worley and Wilson (1996); Murphy et al. (1997); Wallis et al. (2003)

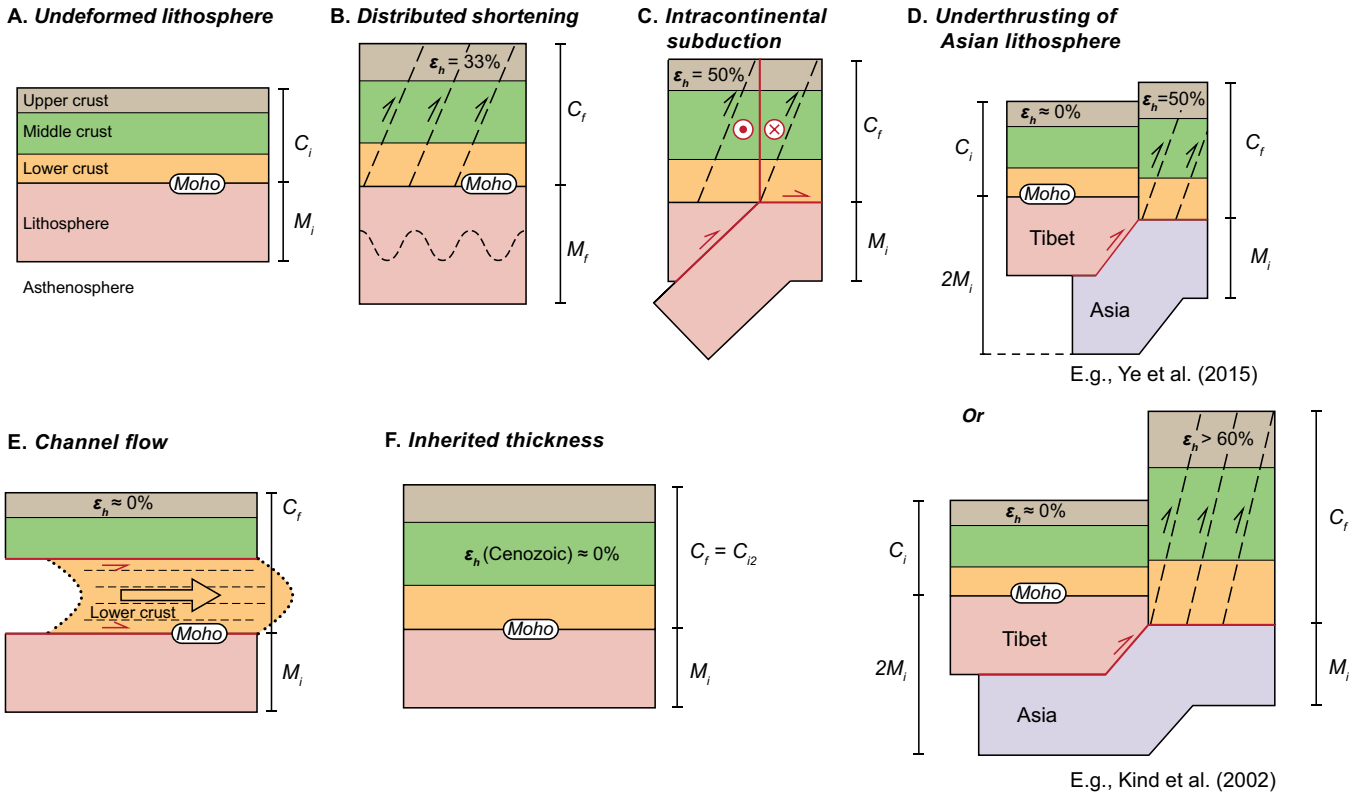

Figure 2. Competing end-member models for the development of the northeastern Tibetan Plateau. C_i and C_f represent the initial and final thickness of the crust, respectively, and M_i and M_f represent the initial and final thickness of the mantle lithosphere, respectively (see text). Red lines indicate major detachment surfaces or strike-slip faults. (A) Continental lithosphere prior to deformation. (B) The distributed shortening model predicts vertically uniform strain, evenly spaced thrust faults, and pure shear thickening of the entire continental lithosphere. (C) The intracontinental subduction model requires subduction of the mantle lithosphere, which is decoupled from the deforming crust. The concentrated mixed-mode deformation (i.e., left-slip and thrust faulting) and subduction occur along older suture zones. (D) The underthrusting model predicts crustal shortening at the plateau margins to accommodate southward motion of the Asian mantle lithosphere: strain at this margin is either large (>60% strain) if the Asian mantle lithosphere is underthrust to central Tibet (e.g., Kind et al., 2002) or more minor (~50% strain) if it is only underthrust to Qaidam Basin (e.g., Ye et al., 2015). Little crustal shortening should occur away from the plateau margins. (E) The channel flow models predict lateral motion of the lower crust and little shortening in the upper crust. Vertical inflation of a ductile channel leads to thickening of the crustal lithosphere. (F) The present-day thickness may be inherited from an older pre-Cenozoic collisional event; in this case, the final present-day crustal thickness C_f is equal to the pre-Cenozoic crustal thickness C_{i2}, which was attained during a pre–India-Asia collision thickening process.

Geosphere, published online on 5 February 2016 as doi:10.1130/GES01254.1

This margin is defined by the 350-km-wide and 1300-km-long Qilian Shan–Nan Shan thrust belt (Molnar and Tapponnier, 1975; Gaudemer et al., 1995; Meyer et al., 1998; Yin and Harrison, 2000; Taylor and Yin, 2009), which occupies about one-fifth of the Tibetan-Himalayan orogen and is one of the widest active thrust belts in the India-Asia collisional zone (Fig. 1) (Yin, 2010). The absence of detailed structural observations, including systematic geologic mapping and subsurface seismic data, inhibits our understanding of plateau growth mechanisms. The timing and magnitude of deformation in this region, which is located more than 1500 km north of the India-Asia collisional front (Fig. 1), has implications for strain transfer and partitioning across the Tibetan-Asian lithosphere (e.g., Wang et al., 2011; Yuan et al., 2013).

Here we investigate the magnitude of shortening across the northern Qilian Shan frontal thrust system and the adjacent Hexi Corridor foreland by integrating surface geology and subsurface data. The Hexi Corridor is rich in petroleum resources (e.g., Wang and Coward, 1993; Chen and Yang, 2010; He and Pang, 2013) and has been surveyed extensively by seismic reflection profiling (e.g., J. Wu et al., 2006; Yang et al., 2007a, 2007b). We acquired and interpreted three seismic reflection profiles to estimate horizontal strain by constructing and restoring balanced cross sections that adhere to the known surface geology and regional tectonic history. We use our strain estimates together with other published shortening estimates across northern Tibet (Fig. 3; Table 2) to evaluate plateau construction mechanisms. Specifically, our results suggest that the Qilian Shan frontal thrust system has absorbed a minimum of 53% north-south Cenozoic shortening, which was accommodated by the north-directed thrust faults that place Mesozoic and Paleozoic rocks over Cenozoic sediments. Our estimated strain magnitudes are comparable to the results of a seismic reflection study ~450 km to the east (Gao et al., 2013) but higher than those obtained within the Qilian Shan–Nan Shan from surface geologic mapping alone (~5%–30% strain) (e.g., Gaudemer et al., 1995; Meyer et al., 1998; Lease et al., 2012; Craddock et al., 2014) (Fig. 3). This discrepancy may be due to a combination of factors. First, this may highlight the limitations of some existing regional structural studies, including the tendency for the actual shortening to

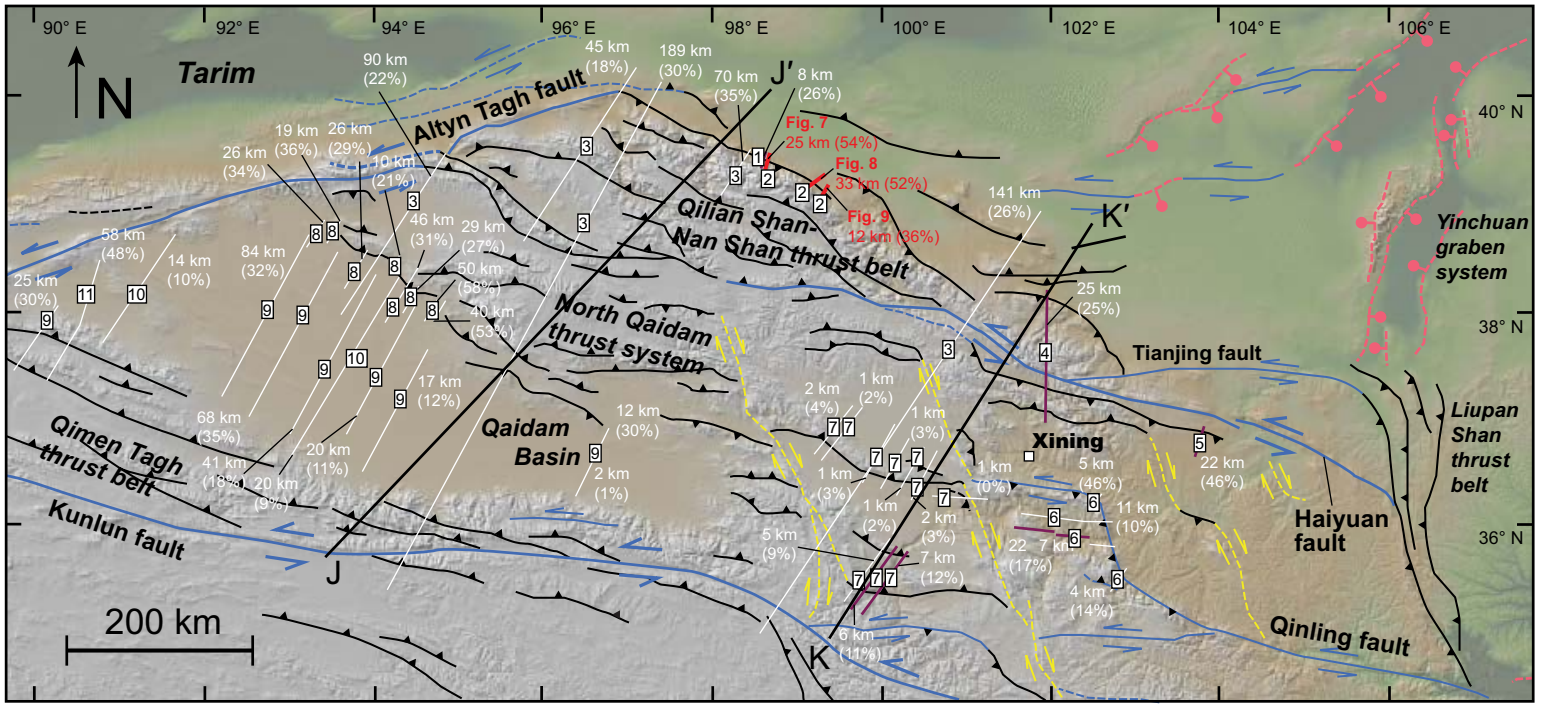

Figure 3. Simplified Cenozoic fault map of the northeastern Tibetan Plateau showing the existing shortening estimates that are compiled in Table 2. Purple section lines correspond to cross sections and shortening estimates that are shown as examples in Figure 4. Red lines show the three seismic profiles analyzed in this study, with corresponding strain estimates. Symbols are as in Figure 1. For figure clarity some sections and shortening estimates from the North Qaidam thrust system (Yin et al., 2008a) have been omitted. The boxed numbers correspond to the reference for each shortening strain estimate: 1—Zheng et al. (2010), 2—this study, 3—Meyer et al. (1998), 4—Gaudemer et al. (1995), 5—Gao et al. (2013), 6—Lease et al. (2012), 7—Craddock et al. (2014), 8—Yin et al. (2008a), 9—Yin et al. (2008b), 10—Zhou et al. (2006), 11—Yin et al. (2007a). Section lines J–J′ and K–K′ correspond to the crustal thickness and shortening magnitude relationship explored in Figure 11.

Geosphere, published online on 5 February 2016 as doi:10.1130/GES01254.1

TABLE 2. EXISTING CROSS SECTIONS AND SHORTENING ESTIMATES ACROSS NORTHERN TIBET

Location	Section label*	Orientation	Shortening (km)[strain %]	Restored length (km)	T_i† (km)	Reference
Qilian Shan-Nan Shan thrust belt						
North	A–A′	NE–SW	8.2 [26]	31.3	41–52	Zheng et al. (2010)
North	S–S′	NNE–SSW	25 [54]	46	23–29	This study
	T–T′	NNE–SSW	33 [53]	64	26–34	
	U–U′	NNE–SSW	12 [36]	33	35–45	
Regional	b	NE–SW	90 [22]	415	43–55	Meyer et al. (1998)
	d	NE–SW	35–45 [13–18]	258–268	46–59	
	f	NE–SW	50–70 [23–35]	200–220	39–50	
	Composite b, d, f	NE–SW	150 [31]	485	38–48	
	C1	NE–SW	188.5 ± 98 [30]	630	39–49	
	C2	NE–SW	141 ± 84 [26]	540	41–52	
	Mass balance	NE–SW	120 ± 30 [14–23]	640	45–57	
Regional	–	NE–SW	360 [50]	710	28–35	Yin and Harrison (2000)
East	A–A′	NNW–SSE	25 [25]	100	41–53	Gaudemer et al. (1995)
Baiyin thrust	Baiyin thrust§	NNW–SSE	22.3 [46]	47.9	30–38	Gao et al. (2013)
Jishi Shan	A–A′	W–E	14.3 [14.2]	100.6	47–60	Lease et al. (2012)
	B–B′	W–E	10.5 [10.4]	100.8	49–63	
	C–C′	W–E	8.4 [26]	32.4	41–52	
West Qinling	D–D′	NE–SW	4.3 [14.2]	30.3	47–60	Lease et al. (2012); Clark et al. (2010)
Laji Shan	E–E′	NE–SW	5.1 [46]	11.1	30–38	Lease et al. (2011, 2012)
Qinghai Nan Shan	a	NNE–SSW	2.2 [4.2]	52.2	53–67	Craddock et al. (2014)
	b	NNE–SSW	0.8 [1.6]	50.8	54–69	
	c	NNE–SSW	1.4 [2.7]	51.4	54–68	
	d	NNE–SSW	1.3 [2.5]	51.3	54–68	
	e	NNE–SSW	0.9 [1.8]	50.9	54–69	
	f	NNE–SSW	1.6 [3.1]	51.6	53–68	
	g	W–E	0.8 [0]	32.3	55–70	
Gonghe Nan Shan	a	NE–SW	5.1 [9.3]	55.1	50–63	Craddock et al. (2014)
	b	NE–SW	6.4 [11.3]	56.4	49–62	
	c	NE–SW	6.9 [12.1]	56.9	48–62	
North Qaidam thrust system						
North Qaidam	(1)	NE–SW	26 [34]	60	36–46	Yin et al. (2008a)
	(2)	NE–SW	19 [36]	53	35–45	
	(3)	NE–SW	26 [29]	91	39–50	
	(4)	NE–SW	10 [21]	48	43–55	
	(5)	NE–SW	46 [31]	149	38–48	
	(6)	NE–SW	29 [27]	103	40–51	
	(7)	NE–SW	50 [58]	86	23–29	
	(8)	NE–SW	40 [53]	68	26–33	
	Gaoquan	NE–SW	9.8 [63]	15.6	20–26	
	Lulehe	NE–SW	31 [63]	49	20–26	
	Luliang Shan	NE–SW	34 [55]	62	25–32	
	Gaqiu	NE–SW	22 [38]	57.5	34–43	
	Xiaoqaidam	NE–SW	6.5 [23]	33.5	42–53	
	Lenghu-4	NE–SW	1.6 [35]	4.6	36–46	
	Lenghu-4	NE–SW	16 [39]	41	34–43	
Qaidam Basin thrust system						
Qaidam Basin	1	NE–SW	84 [32.3]	257	37–47	Yin et al. (2008b)
	2	NE–SW	68 [35.1]	270	36–45	
	3	NE–SW	41 [17.7]	231	45–58	
	4	NE–SW	20 [10.7]	187	49–63	
	5	NE–SW	17 [12.1]	147	48–62	
	6QB	NE–SW	2 [1]	52	54–69	
	6QS	NE–SW	12 [30]	40	39–49	
Qaidam Basin	2	NE–SW	13.74 [9.6]	143.06	50–63	Zhou et al. (2006)
	6 + 9	NE–SW	19.98 [9]	219.82	50–64	
Qimen Tagh thrust belt						
West	7	NE–SW	25 [30]	74	39–49	Yin et al. (2008b)
West	A–D	NE–SW	58 [48]	120	29–36	Yin et al. (2007a)
West	–	NE–SW	270 [57]	470	24–30	Yin and Harrison (2000)

*As reported in original reference.
†Apparent initial predeformational crustal thickness given shortening estimate.
§Restoration above regional Paleozoic unconformity.

Geosphere, published online on 5 February 2016 as doi:10.1130/GES01254.1

be underestimated by surface-based studies that miss hidden structures (e.g., detachments, blind faults, and duplexes). Second, there may be a real difference in strain magnitude between the plateau margin and within the northern plateau interior, suggesting mixed plateau formation processes. By integrating our estimates with existing studies, we propose that the following mechanisms are operating in northern Tibet: (1) southward underthrusting of Asian mantle lithosphere by 200–250 km results in high strain (>53%) along the northern Qilian Shan thrust system, and (2) 250–350 km of distributed crustal shortening throughout the Qaidam Basin, North Qaidam, and Qilian Shan–Nan Shan thrust belts (>30%–45% strain) (Fig. 1) leads to pure shear crustal thickening.

REGIONAL GEOLOGY

The high elevation (~5 km) of the Tibetan Plateau (Fielding et al., 1994) was created in the Cenozoic, as a result of the India-Asia collision (Yin and Harrison, 2000; Tapponnier et al., 2001; Royden et al., 2008), or in the Mesozoic, as suggested for the southern and possibly eastern portions of Tibet (e.g., Worley and Wilson, 1996; Murphy et al., 1997). The average elevation of the northeastern plateau is slightly lower (~4.5 km) and this high topography drops off rapidly to <1.5 km to the northeast in the Hexi Corridor foreland (Fig. 1D). The present-day Qilian Shan–Nan Shan is composed of northwest-trending thrust-bounded ranges and intermontane basins spaced at 30–40 km (Fig. 1B). Crustal thickness estimates across this area range from 55 to 65 km (Fig. 1C) as constrained by receiver function (Yue et al., 2012; Ye et al., 2015), seismic refraction (Zhao et al., 2001), and seismic reflection (Gao et al., 2013) studies. The Ordos Basin, northeast of the Hexi Corridor (Fig. 1B), has far fewer earthquakes than the adjacent plateau and thus is considered a relatively stable block with an average crustal thickness of ~42 km (Chen et al., 2005; Liu et al., 2006; Pan and Niu, 2011).

The Cenozoic Qilian Shan–Nan Shan thrust defines the northeastern margin of the Tibetan Plateau, more than 1500 km to the north of the Himalayan collision front, between North China to the north and Qaidam Basin to the south (Fig. 1). The thrust belt is constructed in a region that had a complex pre-Cenozoic history involving multiple phases of Proterozoic basement deformation, early Paleozoic orogeny, and Jurassic–Cretaceous extension (e.g., Vincent and Allen, 1999; Gehrels et al., 2003a, 2003b; Yin and Harrison, 2000; Yin et al., 2007b).

Early Paleozoic Qilian Orogen and Related Basement Rocks

The Qilian orogen records the early Paleozoic closure of the Qilian Ocean as the Kunlun-Qaidam terrane collided against the southern margin of the North China craton (Yin and Nie, 1996; Şengör and Natal'in, 1996; Sobel and Arnaud, 1999; Yin and Harrison, 2000; Gehrels et al., 2003a, 2003b; Yin et al., 2007b; Xiao et al., 2009; Song et al., 2013). The Qilian orogen is composed of Silurian flysch sequences, Ordovician–Silurian plutonic bodies and arc-type assemblages, ophiolitic mélange, and low- to high-grade metamorphic rocks. The distribution of ophiolitic material indicates that a Cambrian–Ordovician Qilian Ocean separated Qaidam and North China (Smith, 2006; Xiang et al., 2007; Tseng et al., 2007; Zhang et al., 2007; Xia and Song, 2010; Song et al., 2013). The convergence of these continents was facilitated by middle Cambrian–Ordovician subduction and related arc magmatism (Qian et al., 1998; Cowgill et al., 2003; Gehrels et al., 2003a; Su et al., 2004; C. Wu et al., 2004, 2006, 2010; Hu et al., 2005; Y.J. Liu et al., 2006; Quan et al., 2006; He et al., 2007; Tseng et al., 2009; Dang, 2011; Xia et al., 2012; Xiong et al., 2012; Song et al., 2013); intracontinental deformation and ocean closure occurred in Late Ordovician–Silurian time (Song et al., 2006; Y.J. Liu et al., 2006; Zhang et al., 2007; Lin et al., 2010). The orogen is an important preexisting weakness that may have controlled Cenozoic structures in northern Tibet: the present-day Qilian Shan thrust belt and Haiyuan left-slip fault closely follow the trace of the orogen and suture (Fig. 1B) (Taylor and Yin, 2009).

Jurassic and Cretaceous Extensional Setting

The Mesozoic closure of the Paleo-Tethys and Meso-Tethys Oceans (Pullen et al., 2008; Zhang et al., 2014) and associated with slab rollback to the south may have led to regional extension that affected much of the continent to the north, including the Altyn Tagh range, Qaidam Basin, Qilian Shan–Nan Shan, and Hexi Corridor, from southwest to northeast, respectively (Fig. 1) (Huo and Tan, 1995; Vincent and Allen, 1999; Chen et al., 2003; Yin et al., 2008a, 2008b). This extension is expressed by the development of extensive Jurassic and Cretaceous extensional and transtensional basins in the Altyn Tagh range, Qaidam Basin, the Hexi Corridor, and North China (Vincent and Allen, 1999; Chen et al., 2003; Yin et al., 2008a, 2008b). Although no extensional faults have been documented at the surface in the northern Qilian Shan, Jurassic and Cretaceous strata are widespread and record a transition from marginal marine and lacustrine to mostly terrestrial sedimentation. Jurassic strata consist of sandstone interbedded with siltstone, carbon-rich shale, and coal (Gansu Geological Bureau, 1989; Qinghai BGMR, 1991). Upper Jurassic beds are often lacustrine. Cretaceous terrestrial red beds that fine upward from coarse sandstone to lacustrine deposits that are prominently exposed along many basins in northern Tibet, from the Xining Basin in the south to the Hexi Corridor in the north (Fig. 1B) (Horton et al., 2004; Pan et al., 2004).

Cenozoic Structures

Cenozoic shortening in northern Tibet is accommodated in the northwest-trending Qilian Shan, North Qaidam, and Qimen Tagh thrust belts (Jolivet et al., 2003; Yin et al., 2007a, 2008a, 2008b), from north to south, respectively (Fig. 1B). These major thrust belts link with the active >1000-km-long east-striking Haiyuan, Qinling, and Kunlun left-slip faults (Fig. 1B) (e.g., Taylor and Yin, 2009). The Haiyuan fault and ~350-km-wide Qilian Shan–Nan Shan thrust belt

Geosphere, published online on 5 February 2016 as doi:10.1130/GES01254.1

define the northeastern margin of the Tibetan Plateau, and the Hexi Corridor foreland basin bounds the plateau to the northeast (Fig. 1B). Thrusting initiated locally at 50–45 Ma in the southern Qilian Shan–Nan Shan and North Qaidam thrust belts, and deformation migrated southward to the Qimen Tagh and northward to the northern Qilian Shan thrust belts by 25–20 Ma (Mock et al., 1999; Jolivet et al., 2001; Dupont-Nivet et al., 2004; Horton et al., 2004; Yin et al., 2008a, 2008b; Clark et al., 2010; Duvall et al., 2011). The region underwent a major pulse of deformation marked by the development of left-slip fault systems by 20–15 Ma (Jolivet et al., 2001; Craddock et al., 2011; Duvall et al., 2013; Yuan et al., 2013). Along the outer plateau margins, thrust initiation occurred at 10–8 Ma (Zheng et al., 2006, 2010; Godard et al., 2009).

Inversion of the global positioning system (GPS) velocity field across the region yields a N30°E contractional strain field (Zhang et al., 2004; Allmendinger et al., 2007). GPS velocity differencing between North China and Qaidam Basin suggests overall north-south convergence rates of ~5.5 mm yr^{-1} across the Qilian Shan–Nan Shan thrust belt (Zhang et al., 2004). Fault slip and shortening rates across the Qilian Shan–Nan Shan thrust belt range from <1 to 5 mm yr^{-1} (Hetzel et al., 2004; W.J. Zheng et al., 2009, 2013; D. Zheng et al., 2010; Champagnac et al., 2010; Yuan et al., 2011; Craddock et al., 2014). The variability and uncertainty of these rates arise because the magnitude of Cenozoic fault offset and total shortening remains poorly constrained throughout most of the Qilian Shan–Nan Shan. A detailed description of existing Cenozoic crustal shortening estimates is discussed herein.

TESTING PLATEAU FORMATION MODELS WITH CRUSTAL SHORTENING ESTIMATES

A combination of mechanisms (Table 1) probably operates to generate the modern Tibetan Plateau (e.g., Molnar et al., 1993; Yuan et al., 2013). Geophysical studies of the lithosphere are valuable to understand geologic processes operating in the subsurface, but indirect observations and nonunique interpretations of detailed structures limit the extent to which hypotheses can be satisfactorily tested (e.g., Ammon et al., 1990; Brown et al., 1996; Makovsky and Klemperer, 1999; Vergne et al., 2002, 2003; Frederiksen et al., 2003; Sherrington et al., 2004). An alternative quantitative approach for distinguishing among plateau construction models is to evaluate the spatial and temporal variations in the magnitude and style of Cenozoic crustal shortening strain via balanced cross-section construction and restoration (Dahlstrom, 1969). Although strain estimates from balanced cross-section restoration can be associated with large uncertainties and the solutions are often nonunique (e.g., Yin, 2006; Yin et al., 2010a; Judge and Allmendinger, 2011), our understanding of thrust systems (Boyer and Elliott, 1982) allows for well-constrained minimum strain estimates that are based on direct field observations (e.g., bedding truncations, fault cutoffs, unit juxtapositions, and fault geometry requirements). These strain estimates place constraints on the vertical thickening and possible outward growth of the plateau.

Tectonic Models and Implications for Shortening along the Tibetan Plateau's Northeastern Margin

Here we briefly summarize the proposed tectonic models for the construction of the Tibetan Plateau (Table 1), including their predictions for the distribution, magnitude, and timing of Cenozoic crustal strain across the Qilian Shan–Nan Shan thrust belt. The distributed shortening model (Fig. 2B) predicts vertically uniform shortening and pure shear thickening of the Asian crust (Dewey and Bird, 1970; Dewey and Burke, 1973) or its entire lithosphere (England and Houseman, 1986). Following the onset of India-Eurasian collision in the south (Zhu et al., 2005; van Hinsbergen et al., 2011), deformation and crustal thickening propagates northward, either steadily throughout the Cenozoic (England and Houseman, 1986) or rapidly with deformation occurring in the north soon after collision (i.e., within millions of years) (e.g., Horton et al., 2002; Yin et al., 2008a, 2008b; Wang et al., 2008; Dayem et al., 2009; Rohrmann et al., 2012). These models predict ~30%–40% shortening strain throughout Tibet to explain the present-day crustal thickness.

Meyer et al. (1998) and Tapponnier et al. (2001) suggested that deformation propagates northward across the plateau in discrete steps. Preexisting Paleozoic and Mesozoic sutures (Fig. 1B) focus deformation in zones of intracontinental subduction that are associated with post–India-Asia collision volcanic belts that also young to the northeast. Furthermore, oblique convergence causes deformation to occur in a mixed mode of thrust and left-slip faulting (Fig. 2C). This concept is supported by the observation that active strike-slip faults follow the trace of Phanerozoic sutures (Fig. 1B) (Taylor and Yin, 2009). Deformation predictions of the intracontinental subduction model include (1) northward-propagating deformation starting in the south in the early Cenozoic and reaching the northeastern margin of the plateau by Pliocene–Quaternary time, (2) focused deformation along Phanerozoic suture zones, and (3) coupled left-slip and oblique thrust faulting (Fig. 2C).

Receiver function analyses suggest that the Asian mantle lithosphere is underthrusting northern Tibet (Fig. 2D). Large-scale underthrusting models (Kind et al., 2002; Zhao et al., 2011) require as much as ~1400 km of crustal shortening (~80% strain) across the 350-km-wide Qilian Shan–Nan Shan thrust belt on the northern margin of the plateau to accommodate such motion of the Asian mantle lithosphere (Fig. 1A), whereas the smaller scale underthrusting models (Feng et al., 2014; Ye et al., 2015) suggest 300 km of shortening (~46% strain). Both iterations of these models involve a southward propagation of structures from the Hexi Corridor foreland and minimal Cenozoic strain in the Qaidam Basin and Qimen Tagh thrust belts to the south (Fig. 1B).

Several groups of models argue that a lateral pressure gradient drives lower crustal channel flow and vertical inflation of the crust (e.g., Zhao and Morgan, 1987; Bird, 1991; Royden et al., 1997, 2008; Clark and Royden, 2000; Clark et al., 2004) (Fig. 2E). These models predict the outward flux of low-viscosity material from the southern and central regions of the plateau and a similar outward propagation of surface uplift. Lateral channel flow should be decoupled from the upper crust so that Cenozoic crustal strain on the plateau

Geosphere, published online on 5 February 2016 as doi:10.1130/GES01254.1

surface must be minimal (<5%) and the upper crust undergoes only vertical motion (Fig. 2E). Although the channel flow model of Clark and Royden (2000) only predicts crustal flow in eastern Tibet and does not specifically refer to the Qilian Shan, the overall channel-flow process (Zhao and Morgan, 1987; Bird, 1991; Royden et al., 2008) should be considered as a general mechanism for thickening and thinning of the Tibetan crust.

Although most of the present-day topography of the Tibetan Plateau (Fig. 1) was likely created in the Cenozoic as a result of the India-Asia collision (Yin and Harrison, 2000; Tapponnier et al., 2001; Royden et al., 2008), several regions inherited their crustal thickness from older collisional events (e.g., Worley and Wilson, 1996; Murphy et al., 1997). Based on the regional tectonic history, pre-Cenozoic crustal thickening in northern Tibet could have occurred either during the early Paleozoic Qilian orogen (e.g., Yin and Harrison, 2000; Gehrels et al., 2003a, 2003b; Xiao et al., 2009; Song et al., 2013) or as a result of far-field uplift during the latest Paleozoic–early Mesozoic collisions between North China and South China or Qiantang and Asia (e.g., Yin and Nie, 1993; Pullen et al., 2008). If either case is correct, topography in the region must have persisted until today (Fig. 2F), the majority of deformational structures should be pre-Cenozoic, and erosion must be minimal over a period of hundreds of millions of years.

Existing Shortening Estimates across the Qilian Shan–Nan Shan Thrust Belt

A compilation of existing Cenozoic shortening estimates across northern Tibet (Fig. 3) are listed in Table 2. Gaudemer et al. (1995) constructed a north-northwest–trending cross section in the eastern Qilian Shan based mainly on interpreted satellite images and existing regional geologic maps (Fig. 3 and 4A); their cross section (Fig. 4A) involves south-dipping thrust faults that sole into a 10°–20° south-dipping detachment surface that merges with the Haiyuan fault at ~25 km depth. Gaudemer et al. (1995) estimated a minimum of 25 km shortening of a section that has a restored length of 100 km (~25% strain) by restoring the unconformity overlying early Paleozoic and older basement rocks back to subhorizontal (Fig. 4A). By using a regionally correlative marker horizon (i.e., the Paleozoic unconformity surface), strain within the pre-Cenozoic strata can be considered. Although the cross section is located near the Haiyuan fault (Fig. 3), out-of-plane motion (i.e., parallel to the Haiyuan fault) is unconstrained on the mapped faults.

The shortening estimates presented by Meyer et al. (1998) (Fig. 3) are based on two independent methods (Table 2). First, they developed several serial north-northeast–trending cross sections across the western Qilian Shan–Nan Shan (Fig. 3) using satellite image analysis with minor field checks. The restoration of Cretaceous and Cenozoic marker horizons yields 20%–30% shortening strain with an overall minimum of 150 km north-south shortening (>31% strain) across the entire Qilian Shan–Nan Shan thrust belt. Second, Meyer et al. (1998) derived bulk shortening estimates of 120 ± 30 km (Table 2) from a regional mass balance of eroded sediments, assuming isostatic compensation and an initial crustal thickness of 47.5 km. Meyer et al. (1998) noted that an unconstrained left-slip component on strike-slip faults (i.e., the Qinling and Haiyuan faults) adds uncertainties to their estimates.

In the northern Qilian Shan, adjacent to our study area, Zheng et al. (2010) used apatite (U-Th)/He (AHe) data (Fig. 3) to show rapid cooling ca. 10 Ma. The preservation of a paleo–partial retention zone (PRZ) in the hanging wall and growth strata in the footwall (Fig. 4C) allowed Zheng et al. (2010) to estimate the horizontal shortening magnitude of 8.2 ± 1.8 km (26% strain) (Fig. 4C) and an average shortening rate of ~1 mm yr^{-1}. These estimates are based on the assumption that shortening was accommodated by a single 30° south-dipping planar thrust (Fig. 4C) initiated ca. 10 Ma. Lease et al. (2012) constrained shortening across the West Qinling thrust fault using existing AHe ages (Clark et al., 2010) to obtain a ca. 110 Ma marker horizon in the footwall and hanging wall. The restoration of this horizon along a single south-dipping fault (average dip of 45°–50°) yields 4.3 km of horizontal shortening of a section that has a restored length of 30.3 km (~14.2% strain). Similarly, AHe ages were used (Lease et al., 2011, 2012) to develop a north-east–trending cross section across the Jishi Shan (Fig. 1B) and to estimate 14.4 km shortening of a section that has a restored length of 100.6 km (~14.2% strain) (Fig. 4B).

A seismic reflection analysis across the eastern Haiyuan fault was conducted by Gao et al. (2013) (Fig. 3); they balanced and restored a 26-km-long section of a 180-km-long seismic reflection profile to estimate Cenozoic strain (Fig. 4D). The section crosses the Baiyin fault, and despite having no kinematic data to determine if it is a thrust or strike-slip fault, Gao et al. (2013) inferred this fault to be a thrust on the basis of its low-angle geometry in cross-section view and an oblique relationship with the left-slip Haiyuan fault in map view (Fig. 1B). Line-length balancing of their cross-section model yielded 22.3 km of shortening across a 25.7-km-long deformed section (~46% strain) (Fig. 4D).

Craddock et al. (2014) presented 10 line-length balanced north-south cross sections across the Qinghai and Gonghe Nan Shan, south of Qinghai Lake (Fig. 3), that are restored by bringing Neogene strata to horizontal (Fig. 4E). They suggested 1.5 ± 0.7 km shortening across the Qinghai Nan Shan. Shortening estimates in the Gonghe Nan Shan to the south are higher, ranging from 5.1 to 6.9 km (6.0 ± 0.9 km). These estimates were coupled with low-temperature thermochronologic and stratigraphic data (Craddock et al., 2011; Zhang et al., 2012) to suggest relatively low north-south shortening rates of ~0.2 mm yr^{-1} and ~0.7 mm yr^{-1} across the Qinghai and Gonghe Nan Shan, respectively.

The diversity in strain and strain rate estimates across the northeastern margin of the plateau (Figs. 3 and 4) may be attributed to both real variations in plateau-construction processes and/or limitations of the balanced cross section restoration method. Due to the remoteness of northern Tibet, many estimates are based primarily on satellite image analysis and reconnaissance-scale surface mapping, which can miss important structures such as blind or hidden faults, detachments, and duplexes. In addition, many studies only consider slip estimates on faults that cut Cenozoic strata and rarely consider deformation of pre-Cretaceous rocks. Especially in the Qilian Shan–Nan Shan thrust belt,

Geosphere, published online on 5 February 2016 as doi:10.1130/GES01254.1

A. Gaudemer et al. (1995)

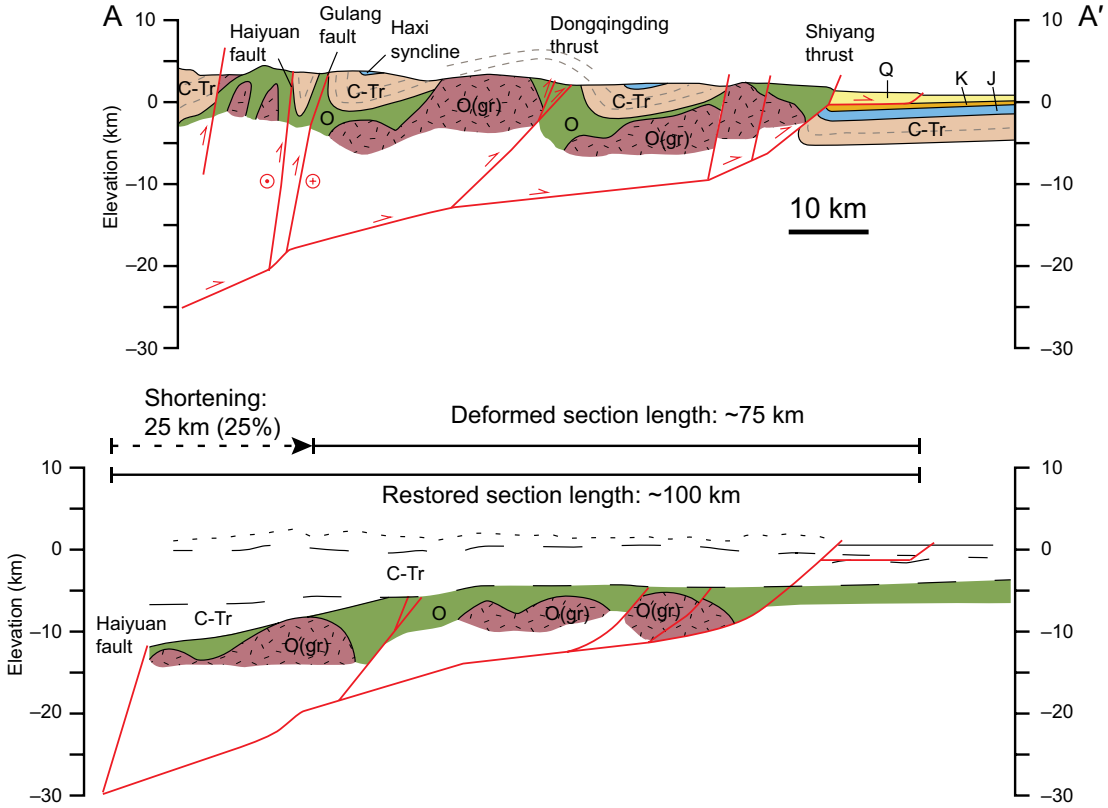

B. Lease et al. (2012)

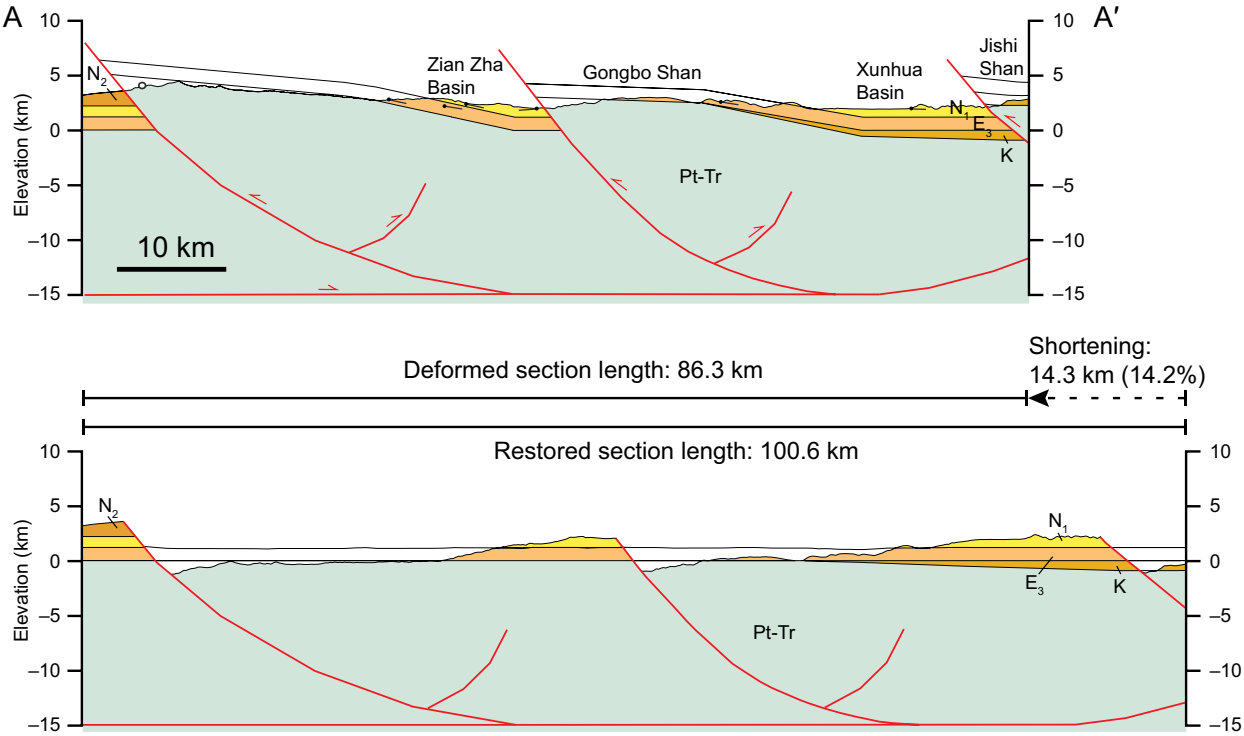

Figure 4 (*on this and following two pages*). Selected examples of existing cross sections and shortening estimates across northern Tibet. Locations are shown in Figure 3. Cross sections were redrafted in original style and modified only to allow comparison among them (e.g., similar-age units are same the same color). (A) Cross section across the eastern Qilian Shan from Gaudemer et al. (1995). Line-length restoration of the section used the base of the Carboniferous strata as a marker horizon and the section was not restored across the left-slip Haiyuan fault. (B) One of three west-east cross sections constructed across the Xunhua Basin–Jishi Shan by Lease et al. (2012). The restoration involved line-length restoration of the base of the Cenozoic strata, and deformation within pre-Cenozoic units is not considered. Note that the depth to detachment and the fault kinematics (oblique versus pure dip slip) on these west-east sections remain unconstrained. For explanation of subscripts 1–3, please see original text of Lease et al. (2012).

Geosphere, published online on 5 February 2016 as doi:10.1130/GES01254.1

C. Zheng et al. (2010)

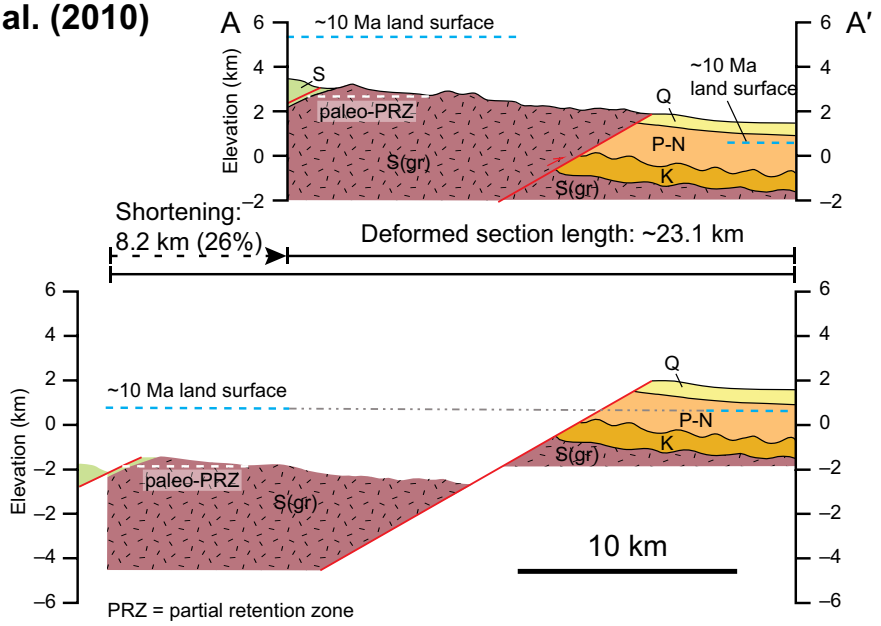

D. Gao et al. (2013)

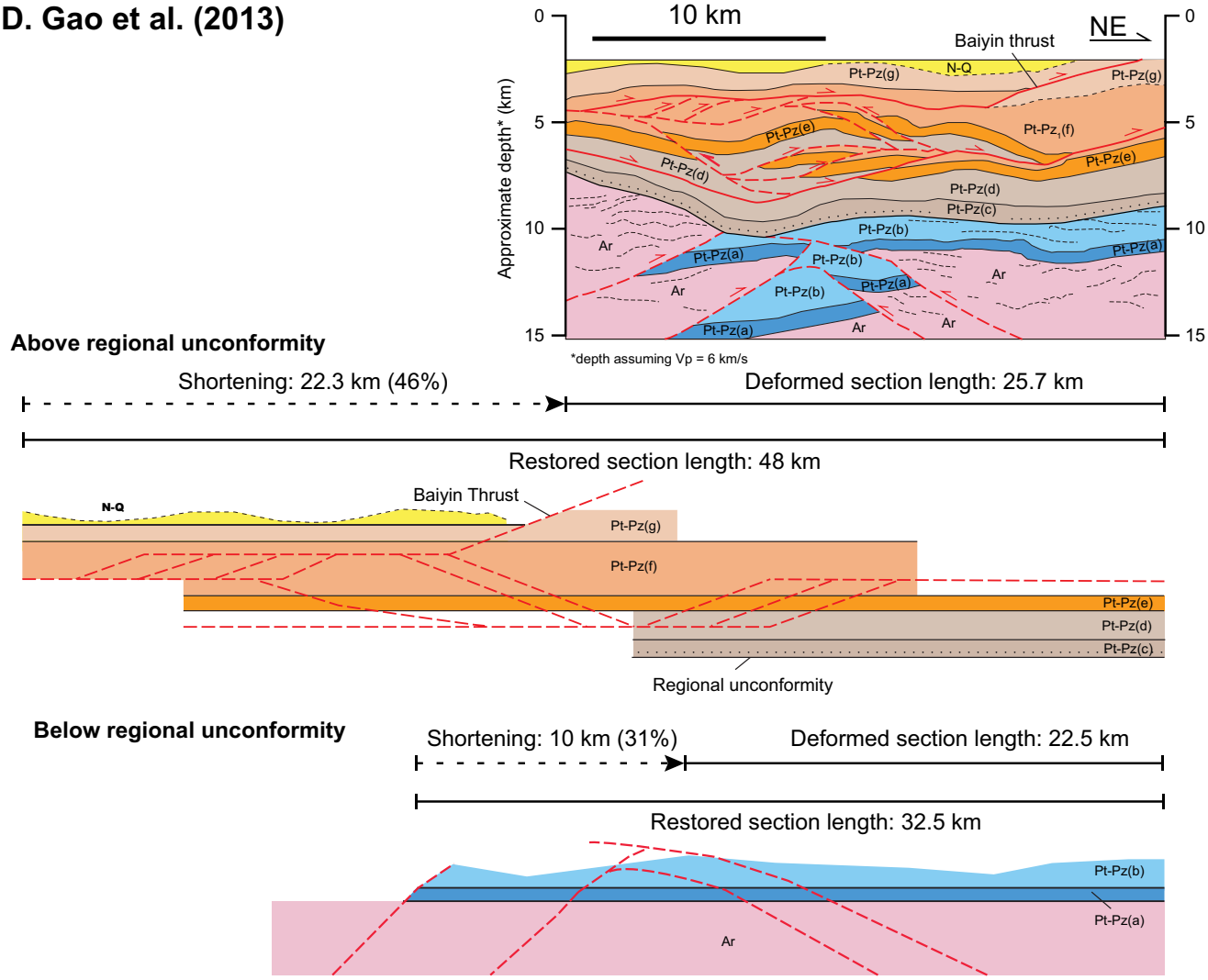

Figure 4 (*continued*). (C) Schematic cross section across the northern Qilian Shan frontal thrust zone by Zheng et al. (2010). The section does not incorporate kinematic data, but restores an apatite helium paleo–partial retention zone (PRZ) in the hanging wall and growth strata in the footwall to constrain vertical fault throw. The assumption of a single fault with a constant dip (30°; Yang et al., 2007a) yields a minimum horizontal shortening estimate. (D) Upper crustal structures associated with the Baiyin thrust from a regional seismic reflection profile obtained by Gao et al. (2013). The interpreted section was constructed by analyzing prominent reflectors and extrapolating surface structures to depth. Note that the depth scale assumes a seismic velocity of 6 km/s throughout the section (e.g., Liu et al., 2006). Line-length restoration of the section, above and below an inferred Paleozoic unconformity, restores prominent reflectors to horizontal. For explanation of subscripts a–g, please see original text of Gao et al. (2013).

Geosphere, published online on 5 February 2016 as doi:10.1130/GES01254.1

E. Craddock et al. (2014)

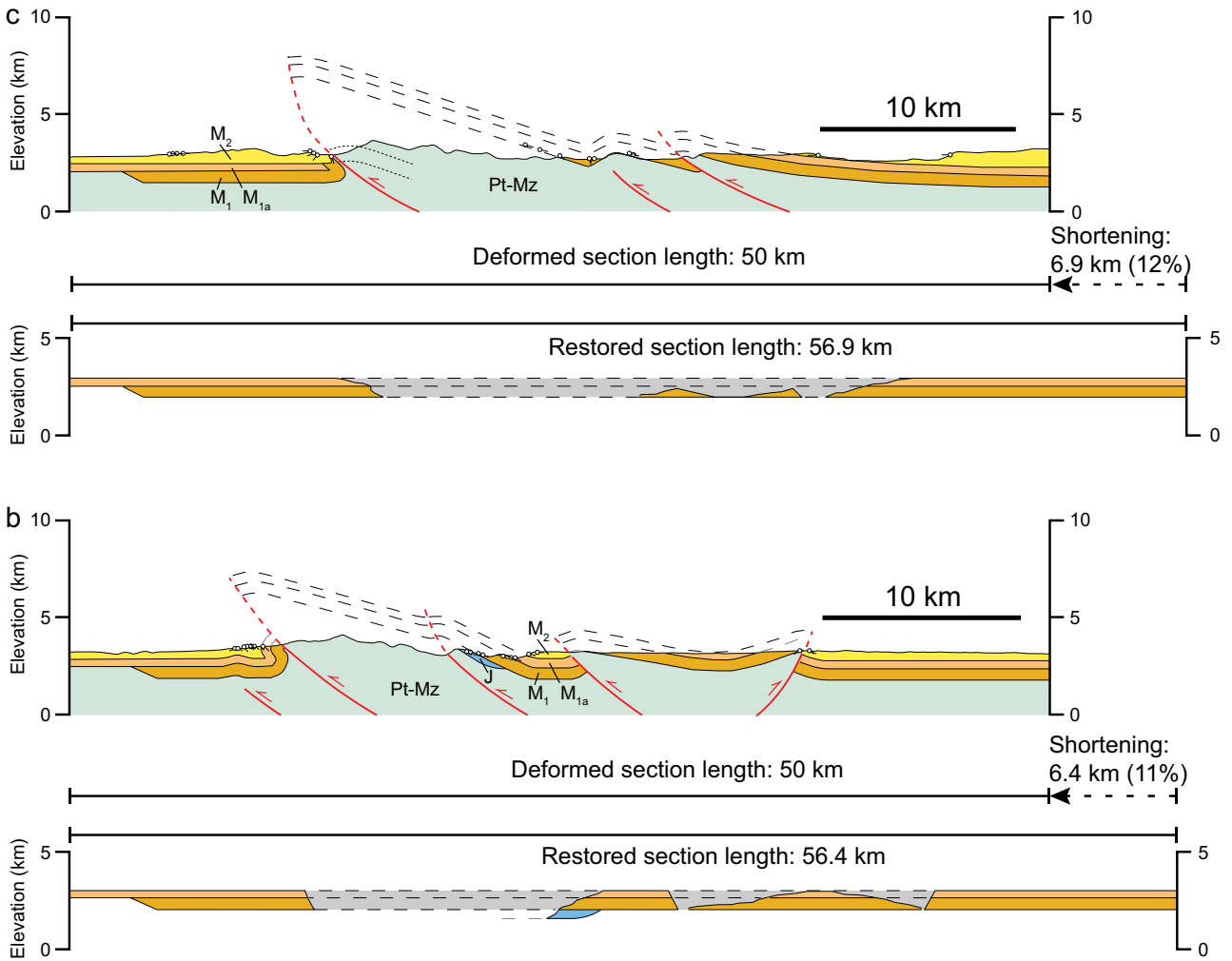

Figure 4 (*continued*). (E) Two of three north-south cross sections across the Gonghe Nan Shan by Craddock et al. (2014). These sections assume that the tilted Cenozoic strata are forelimbs and backlimbs of fault-bend folds. Deformation within pre-Miocene units is not considered. Ar—Archean; C—Carboniferous; E—Eocene; J—Jurassic; K—Cretaceous; Mz—Mesozoic; N—Neogene; O(gr)—Ordovician granite; P—Paleogene; Pt—Proterozoic; Pz—Paleozoic; Q—Quaternary; S—Silurian; Tr—Triassic; Vp—P wave velocity.

Geosphere, published online on 5 February 2016 as doi:10.1130/GES01254.1

where deformation is often thick-skinned and duplicates successions of the early Paleozoic Qilian arc and orogen (e.g., Yin et al., 2007b), much of the Cenozoic strain is recorded as deformation that affects early Paleozoic and older metamorphic rocks. To overcome these issues, an integrated knowledge of subsurface geology and the regional geologic history is required to develop the most reasonable, testable, and restorable geologic cross-section models.

Shortening in Qaidam Basin and the North Qaidam Thrust Belt

The Qaidam Basin and the North Qaidam thrust belts are to the south of the Qilian Shan (Fig. 1B) (Yin et al., 2008a). Balanced cross sections developed primarily from geologic mapping in the North Qaidam thrust belt indicate heterogeneous northeast-southwest crustal shortening that varies from >20% to 60% (Yin et al., 2008a) (Fig. 3; Table 2). In another study, Yin et al. (2008b) used seismic reflection data to develop a series of northeast-trending balanced cross sections across Qaidam Basin that reveal an eastward-decreasing strain gradient, ranging from ~35% strain in the west to >11% in the east (Fig. 3; Table 2). Both of these studies suggest that Cenozoic crustal shortening is the primary mechanism for developing the topography and crustal thickness of Qaidam Basin and the North Qaidam thrust belt.

SEISMIC REFLECTION PROFILES AND BALANCED CROSS SECTIONS

We interpreted three seismic reflection profiles across the northern Qilian Shan frontal thrust system and adjacent foreland that were acquired by the China National Petroleum Company (see Figs. 1 and 5 for their locations) (e.g., J. Wu et al., 2006; Yang et al., 2007a, 2007b). All three uninterpreted high-resolution seismic reflection profiles can be found in Supplemental File 1[1]. First we compiled a regional geologic map from unpublished 1:200,000 scale maps, satellite analysis (i.e., Google Earth and Landsat images), and our own field observations (Fig. 5). The structures imaged in our seismic reflection profiles must be compatible with the local surface geology. Where available, age assignments in the seismic profiles are from drill hole and magnetostratigraphy data (e.g., Yang et al., 1993; Li, 1994; Li and Yang, 1998; Fang et al., 2004; J. Wu et al., 2006; Yang et al., 2007a, 2007b), or surface geology is projected onto the seismic profiles.

Surface Geology in the Northern Qilian Shan

The northern Qilian Shan thrust system and its frontal Yumu Shan thrust ~30 km to the northeast (e.g., Tapponnier et al., 1990) represent the northernmost structures of the Qilian Shan–Nan Shan thrust belt (Fig. 1B). The Yumu Shan is a diverging fault splay (Boyer and Elliott, 1982) that merges with the northern Qilian Shan thrust fault to the southeast (Fig. 1B). These fault systems are bounded to the north by the Hexi Corridor foreland basin (Figs. 1 and 5), which is dissected by several isolated backthrust systems (e.g., the Longshou Shan thrust). The south-dipping Qilian Shan frontal thrust system places Proterozoic–early Paleozoic rocks over the Cenozoic strata of the Hexi Corridor foreland basin (Figs. 5 and 6) (e.g., Li et al., 1998; Fang et al., 2004). Observations of downdip slickenlines and asymmetric folds indicate that the faults are primarily dip-slip thrust faults (e.g., Tapponnier et al., 1990; Reith, 2013). The left-slip Haiyuan fault is located >100 km to the south (Fig. 1) and does not appear to influence the local deformational regime of the northern Qilian Shan.

Hanging-wall rocks are mostly related to the early Paleozoic Qilian orogen, which juxtaposed Proterozoic high-grade gneiss and schist against Ordovician–Silurian low-grade metasediments. It is difficult to determine the age of deformational structures that are mapped entirely within the early Paleozoic units (Fig. 5), and without direct crosscutting relationships or more detailed mapping, these structures may be Paleozoic and/or Cenozoic in age. Ordovician and Silurian strata are often isoclinally folded and bedding is transposed. Early Paleozoic plutons are also widespread throughout the Qilian Shan (e.g., Gehrels et al., 2003a; Song et al., 2013). Two of our seismic profiles cross a >60-km-long Silurian granitoid intrusion, known as the Jinfosi pluton (Zhang et al., 1995), that intrudes Ordovician–Silurian rocks (Gehrels et al., 2003a; Wu et al., 2010) (Fig. 5). This pluton is thrust to the north over Mesozoic–Cenozoic strata and was the focus of a nearby AHe traverse (Zheng et al., 2010) (Fig. 5). The early Paleozoic strata and the plutonic rocks provide no reflective surfaces and are difficult to interpret with seismic reflection analysis because they appear transparent. Because of this issue, our analysis is mostly focused on the geometry of late Paleozoic and younger bedded strata that provide strong reflectors.

Carboniferous (locally Devonian) through Triassic deposits unconformably overlie early Paleozoic rocks (Fig. 5). There are limited surface exposures of Triassic rocks in the study area, and the sedimentary relationship between Late Triassic strata and the overlying Jurassic–Cretaceous sediments is not directly observed in this region. Triassic strata are much more prevalent in the central Qilian Shan–Nan Shan to the southwest (Pan et al., 2004), where the beds are variably subparallel to discordant with the overlying Jurassic–Cretaceous strata. Cretaceous rocks often exhibit a growth strata geometry and are interpreted to have been deposited in extensional grabens (Yin et al., 2008b). Jurassic through Cenozoic strata (Table 3) display the clearest reflectors in our seismic reflection profiles and are most useful for cross-section development. Jurassic rocks consist of coal-rich sandstone and siltstone beds that reach a thickness of ~800–1000 m (Gansu Geological Bureau, 1989; Zhiyi and Dean, 1996). Lower Cretaceous strata are widespread along the northern Qilian Shan and Hexi Corridor, consist of red conglomerate and coarse sandstone, and have a total thickness >2600 m. The more localized upper Cretaceous strata consists of fluvial and lacustrine sandstone that are generally <500 m thick (Zhiyi and Dean, 1996).

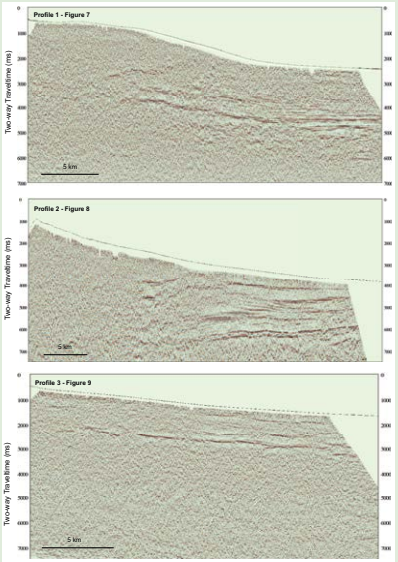

[1]Supplemental File 1. Uninterpreted high-resolution seismic reflection profiles. Please visit http://dx.doi.org/10.1130/GES01254.S1 or the full-text article on www.gsapubs.org to view the Supplemental File.

Geosphere, published online on 5 February 2016 as doi:10.1130/GES01254.1

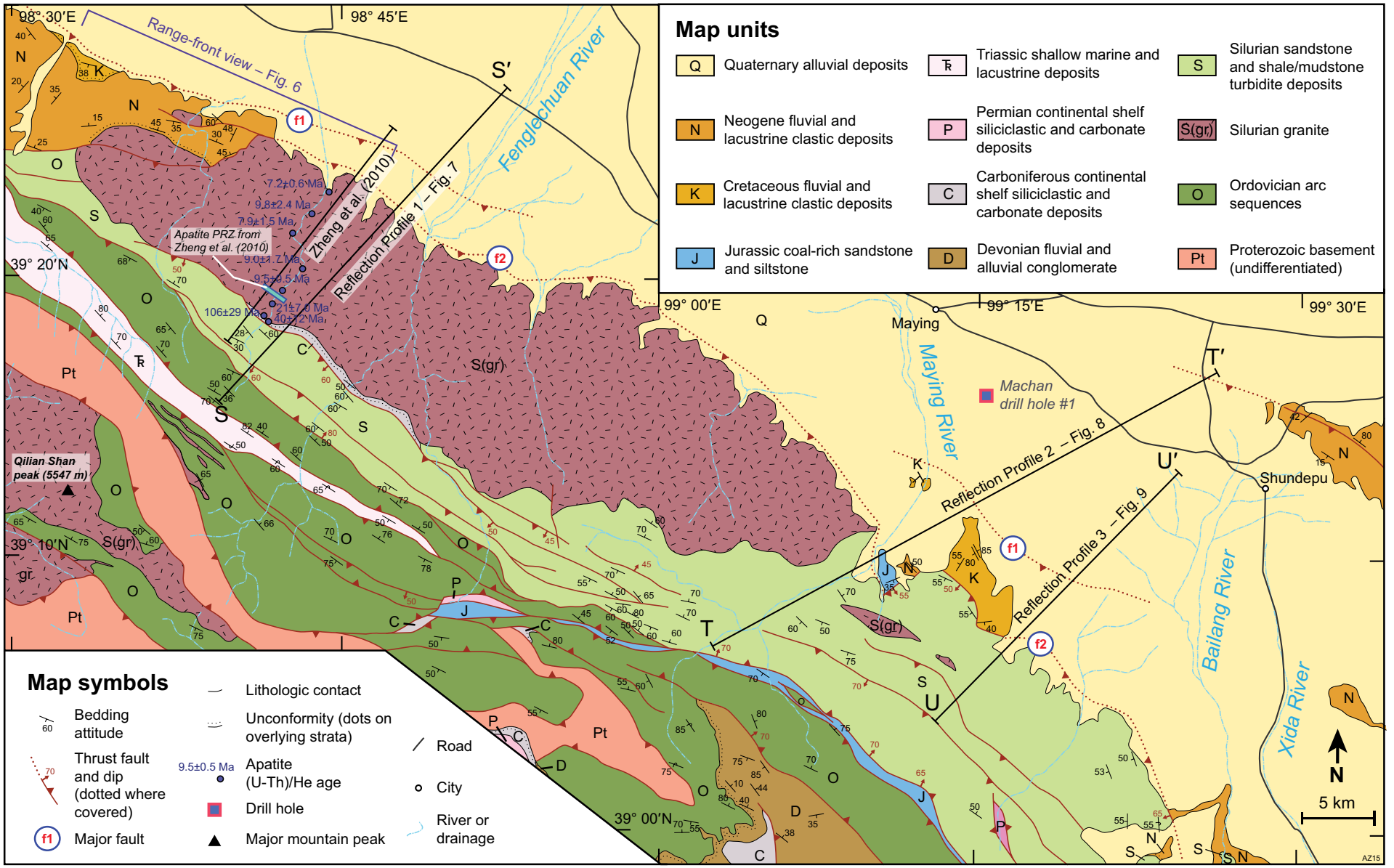

Basemap: 1:200,000 Soviet Military Topographic Map Projection: Gauss-Krasovskii based on Pulkovo 1942 datum Krasovskii spheroid

Figure 5. Geologic map across the northern Qilian Shan frontal thrust zone compiled from unpublished maps, Gansu Geological Bureau (1989), Qinghai BGMR (1991), and our own structural interpretations. See Figure 1 for location. Satellite image viewpoint (Google Earth) of Figure 6 is shown. Also shown are the locations of three seismic reflection profiles (Figs. 7–9), a drill hole described in J. Wu et al. (2006), and the AHe traverse of Zheng et al. (2010). PRZ—partial retention zone.

Geosphere, published online on 5 February 2016 as doi:10.1130/GES01254.1

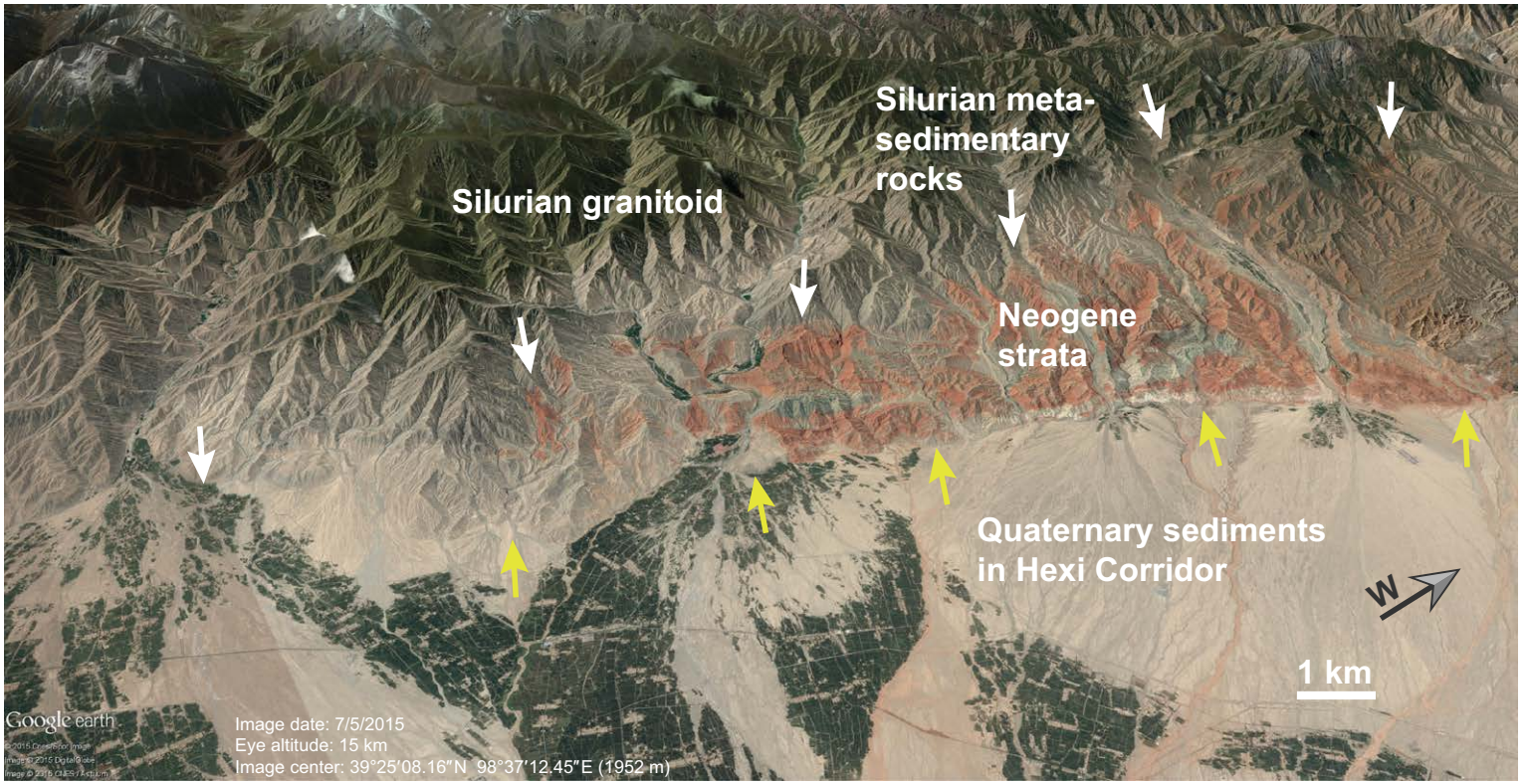

Figure 6. Southward-looking view of Qilian Shan range front from Google Earth. White arrows point to a major thrust fault that juxtaposes Silurian granitoid and metasedimentary rocks against Neogene and Quaternary rocks; the yellow arrows point to a separate thrust fault splay that brings Jurassic–Neogene strata over Quaternary sediments. See Figure 5 for location.

TABLE 3. MESOZOIC AND CENOZOIC STRATIGRAPHY OF THE HEXI CORRIDOR

Unit names	Symbol	Geologic time	Age	Description
Quaternary (undifferentiated)	Q	Quaternary	2.5 Ma to present	Boulders and gravels
Yumen Formation	N_2-Q_1	Pliocene–Pleistocene(?)	ca. 4–2(?) Ma	Pebble to boulder conglomerate with minor sands
Shulehe Formation	N_1	Miocene–Pliocene	23 to ca. 4 Ma	Reddish conglomerate, sandstone, and mudstone
Baiyanghe Formation	P_{E3}	Oligocene	ca. 28–23 Ma	Red-orange sandstone mudstone with gypsum
Huoshaogou Formation	P_{E3}	Oligocene	33.9 to ca. 28 Ma	Red conglomerate, mudstone, and sandstone
Xinminbao Group	K	Cretaceous	145–66 Ma	Red-orange conglomerate and coarse sandstone
Bolou/Dashankou Group	J	Jurassic	201–145 Ma	Coal-rich sandstone and siltstone

Geosphere, published online on 5 February 2016 as doi:10.1130/GES01254.1

The Hexi Corridor foreland is made up of >2.5 km of Cenozoic sediments, mostly Miocene (locally Oligocene) through Pliocene in age (Li et al., 1998; Bovet et al., 2009; Zhuang et al., 2011). The Cenozoic strata are exposed along drainages and localized structural uplifts (e.g., Li, 1993; Bovet et al., 2009). Quaternary sediments are often >1 km thick (Zhang et al., 1990) and consist of alluvial, fluvial, and glaciofluvial deposits (Li and Yang, 1998; Zhao et al., 2002).

Timing of Cenozoic Deformation

Several lines of evidence suggest that contractional deformation and crustal shortening of post-Devonian units across the northern Qilian Shan initiated in the middle Miocene. First, we infer that deformation of Carboniferous through Cretaceous strata occurred in the Cenozoic based on the following observations: (1) thrust faults link with the present-day range-bounding Qilian Shan frontal thrusts (Figs. 5–9), (2) these faults truncate Cenozoic nonmarine deposits and offset Quaternary alluvium (Figs. 5 and 6), (3) regionally, Carboniferous–Triassic strata are conformable and parallel to subparallel, indicating that deformation involving these units was post-Triassic, and (4) Jurassic–Cretaceous strata are extension related (e.g., Vincent and Allen, 1999; Chen et al., 2003; Yin et al., 2008a, 2008b), so contractional deformation of Jurassic–Cretaceous strata must be Cenozoic in age. Second, AHe ages obtained along a nearby traverse (Fig. 5) suggest that rapid cooling across the Qilian Shan frontal thrust system began ca. 10 Ma (Zheng et al., 2010). Lastly, the Cenozoic strata in our seismic reflection profiles, generally Miocene and Pliocene sedimentary rocks, exhibit growth strata relationships with the frontal thrusts (Figs. 7–9).

Approximate Vertical Scale of Seismic Sections and Associated Uncertainties

The vertical axes in the seismic profiles are two-way traveltime, and an approximate depth scale was created assuming an average P-wave velocity of 5.5 km/s (Liu et al., 2006; Gao et al., 2013). Although the use of a single average seismic velocity distorts the geometry of the structures, we assume these effects to be negligible given that the sections are imaging only the uppermost ~15 km of crust and that we are primarily interested in assessing horizontal motion and shortening. The sediment in the foreland may have a lower seismic velocity (e.g., He and Pang, 2013), and therefore our profiles likely overestimate the apparent thickness of Cenozoic sediments. However, our choice of an average seismic velocity leads to very minor uncertainties for our horizontal calculations. If we assume that our approximation of an upper crustal seismic velocity of 5.5 km/s has an associated error of ±0.5 km/s, which is reasonable based on other regional geophysical studies (e.g., Liu et al., 2006) and the global distribution upper crustal p-wave velocities (Christensen and Mooney, 1995), then these uncertainties in the vertical scale affect the actual length of any inclined reflectors. The magnitude of this distortion depends on the apparent dip angle of the reflector. The original length of reflector that dips 45° would be distorted by 3%–4%, whereas more shallowly dipping beds would undergo less elongation. Thus, our line-length balancing analyses of horizontal shortening produce conservative uncertainties of 3%–4%. Our conversion of traveltimes to depth yields apparent bed thicknesses that are consistent with what is observed at the surface (see preceding description), strengthening the validity of our assumption.

Seismic Reflection Profiles

Three seismic reflection profiles (Figs. 7–9) show sequences of finely laminated reflectors, which are interpreted to represent sedimentary strata, and zones of diffuse low reflectivity, which may represent either large plutons or the strongly deformed and transposed Ordovician–Silurian strata. The great density of highly reflective layers allows us to understand the subsurface geometry, and the truncation of these closely spaced reflectors is due to faulting, unconformable deposition, or pluton intrusion. Overall, these three profiles image a south-dipping thrust system involving two major thrust faults that places Paleozoic and older rocks over a relatively undeformed Hexi Corridor foreland to the northeast (Fig. 5). The foreland consists of Mesozoic–Cenozoic sedimentary rocks unconformably overlying older bedded units.

Jurassic strata display the strongest and most continuous reflectors (Figs. 7–9), possibly because of the laterally continuous coal seams in these rocks. These beds generally are 6–8 km below the surface of the Hexi Corridor, but also are exposed along the base of the northern Qilian Shan range (Fig. 5). Cretaceous strata are subparallel to Jurassic strata and also display finely laminated reflectors (Figs. 7–9). Truncations of these reflectors are pronounced and highlight major structures. Growth strata relationships occur in both the Cretaceous and Cenozoic strata; sedimentary rocks thicken to the south-southwest. Sequences of strong reflectors that have apparent thicknesses similar to either the Jurassic or Cretaceous reflectors in the undeformed foreland footwall are interpreted to be the same units in the hanging wall. No clear regional-scale detachment surface at depth is observed in any of the sections, although the hanging-wall and footwall flats are often confined to Cretaceous strata. The transparent granitoid and Ordovician–Silurian units are ambiguous and we refrain from overinterpreting structures within these units. Paleozoic units at depth cannot be subdivided further unless surface extrapolation is possible, and are assigned a general Paleozoic age (Pz).

Seismic reflection profile 1 (Fig. 7) (line S–S′ in Fig. 5) is an ~31-km-long section that images two south-dipping thrusts, which place the Silurian pluton on relatively undeformed Mesozoic–Cenozoic sedimentary rocks in the Hexi Corridor (Fig. 5). The set of strongest reflectors are interpreted to be Jurassic strata (e.g., Yang et al., 1993; Li, 1994; Li and Yang, 1998), 6 km below the surface in the Hexi Corridor (label 1 in Fig. 7), which is conformably overlain by Cretaceous and Cenozoic rocks. Minor north-dipping faults disrupt Jurassic and older strata.

Geosphere, published online on 5 February 2016 as doi:10.1130/GES01254.1

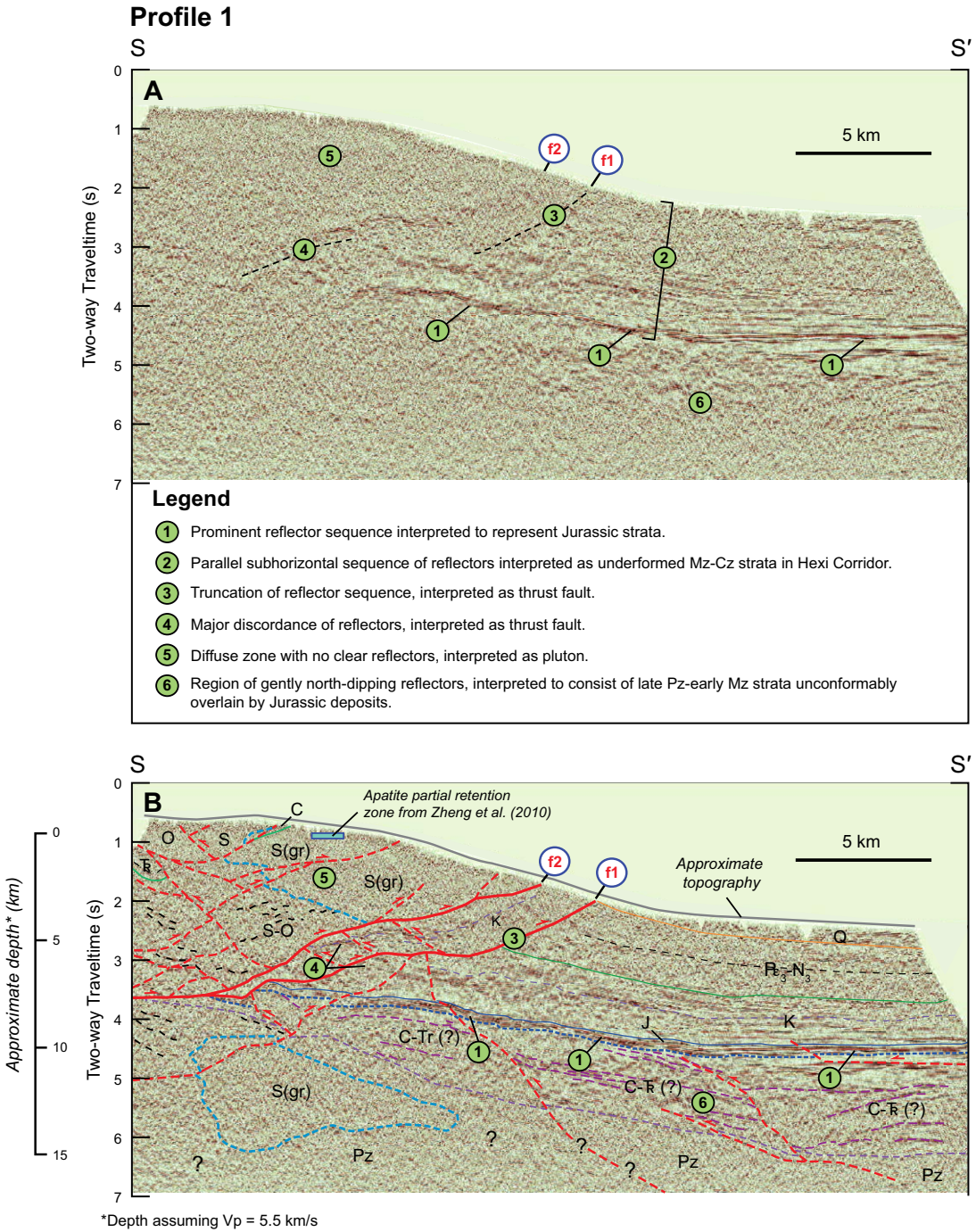

Figure 7 (*on this and following page*). (A) Uninterpreted seismic reflection profile (high-resolution uninterpreted seismic reflection profile can be found in Supplemental File 1). See Figures 1, 3, and 5 for location. Key features, including reflectors and truncations, are labeled from 1 to 6 and described in the legend, and major faults are labeled for discussion in text (i.e., f1 and f2). (B) Interpreted seismic reflection profile. The assigned units are based on projecting surficial geology to depth and well hole and magnetostratigraphy data (e.g., Yang et al., 1993; Li, 1994; Li and Yang, 1998; J. Wu et al., 2006). See Figure 5 for map unit age abbreviations. Important features are labeled as in A. CZ—Cenozoic; Mz—Mesozoic; Pz—Paleozoic.

Geosphere, published online on 5 February 2016 as doi:10.1130/GES01254.1

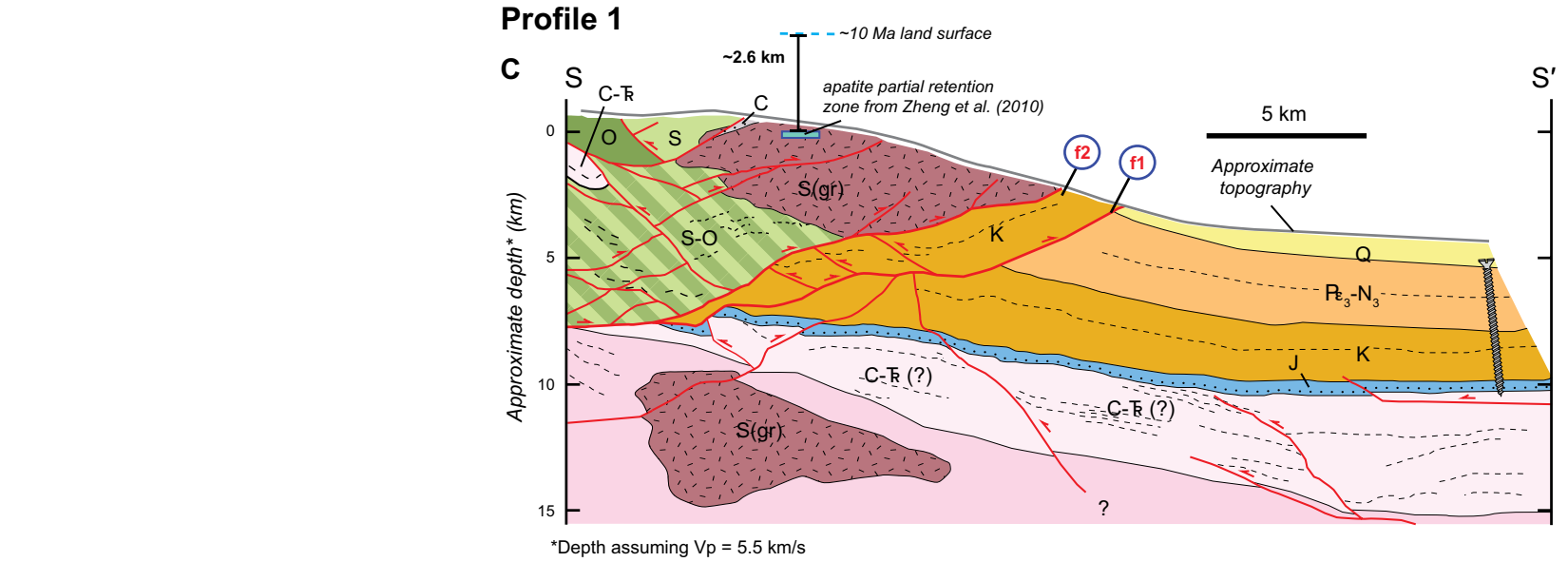

Alternative minimum shortening estimates:
Based on minimum required fault slip: 22 km (53% strain)
Based on restored length of Cretaceous strata (K): 15 km (40% strain)

Figure 7 (*continued*). (C) Geologic cross section based on interpretations shown in B. (D) Restored cross section based on removing slip on imaged faults to move the paleo–partial retention zone (PRZ) and ca. 10 Ma paleoland surface in the hanging wall to a vertically aligned position with the ca. 10 Ma growth-strata surface in the Hexi Corridor footwall. See text for further discussion.

Geosphere, published online on 5 February 2016 as doi:10.1130/GES01254.1

Profile 2

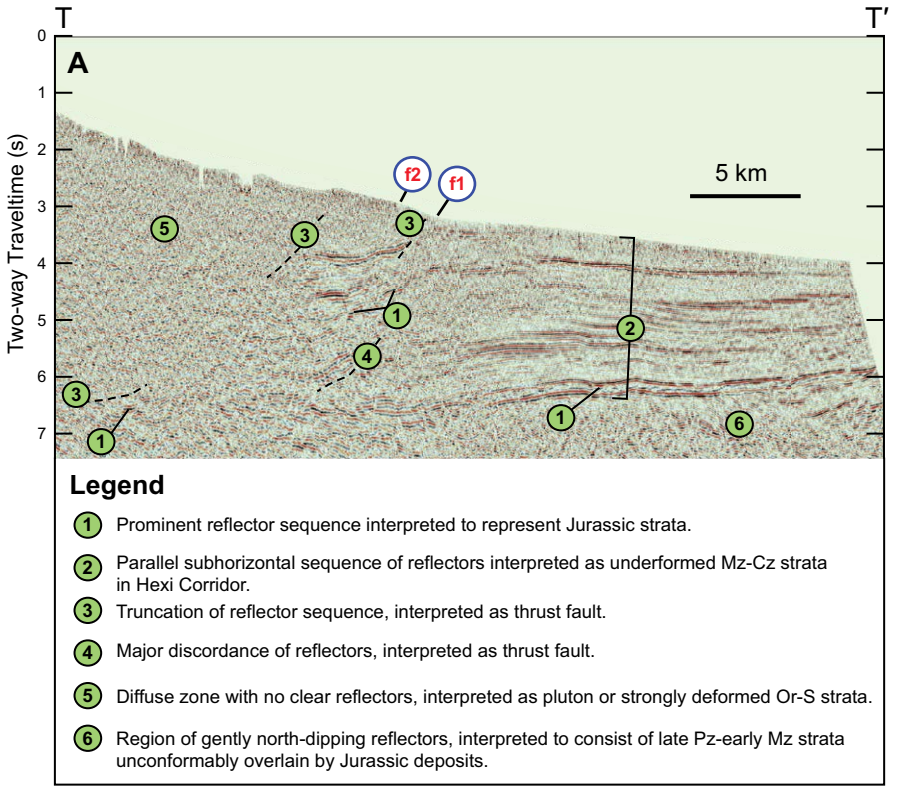

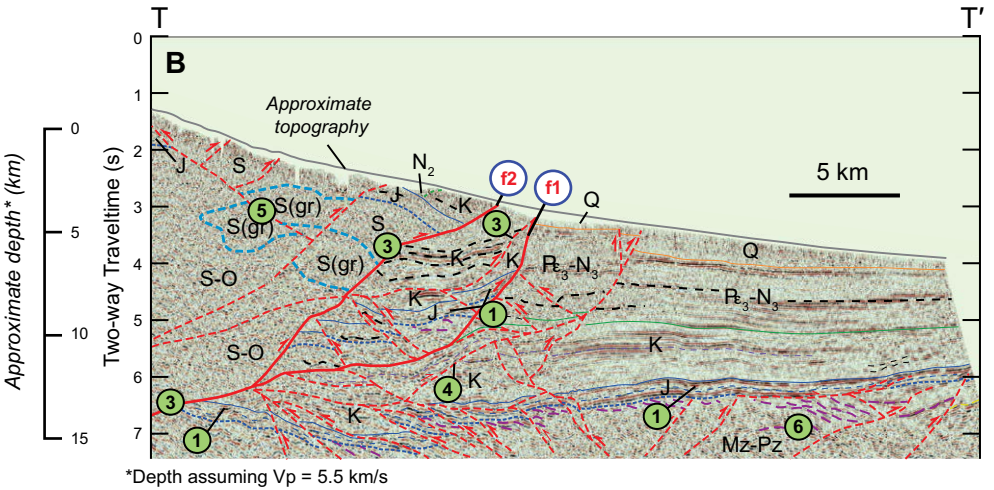

*Depth assuming Vp = 5.5 km/s

Figure 8 (*on this and following page*). (A) Uninterpreted seismic reflection profile (high-resolution uninterpreted seismic reflection profile can be found in Supplemental File 1). See Figures 1, 3, and 5 for location. See Figure 5 for abbreviations. Key features, including prominent reflectors and truncations, are labeled from 1 to 6 and described in the legend, and major faults are labeled for discussion in text (i.e., f1 and f2). (B) Interpreted seismic reflection profile. Important features are labeled as in A. MZ—Mesozoic; Pz—Paleozoic.

Geosphere, published online on 5 February 2016 as doi:10.1130/GES01254.1

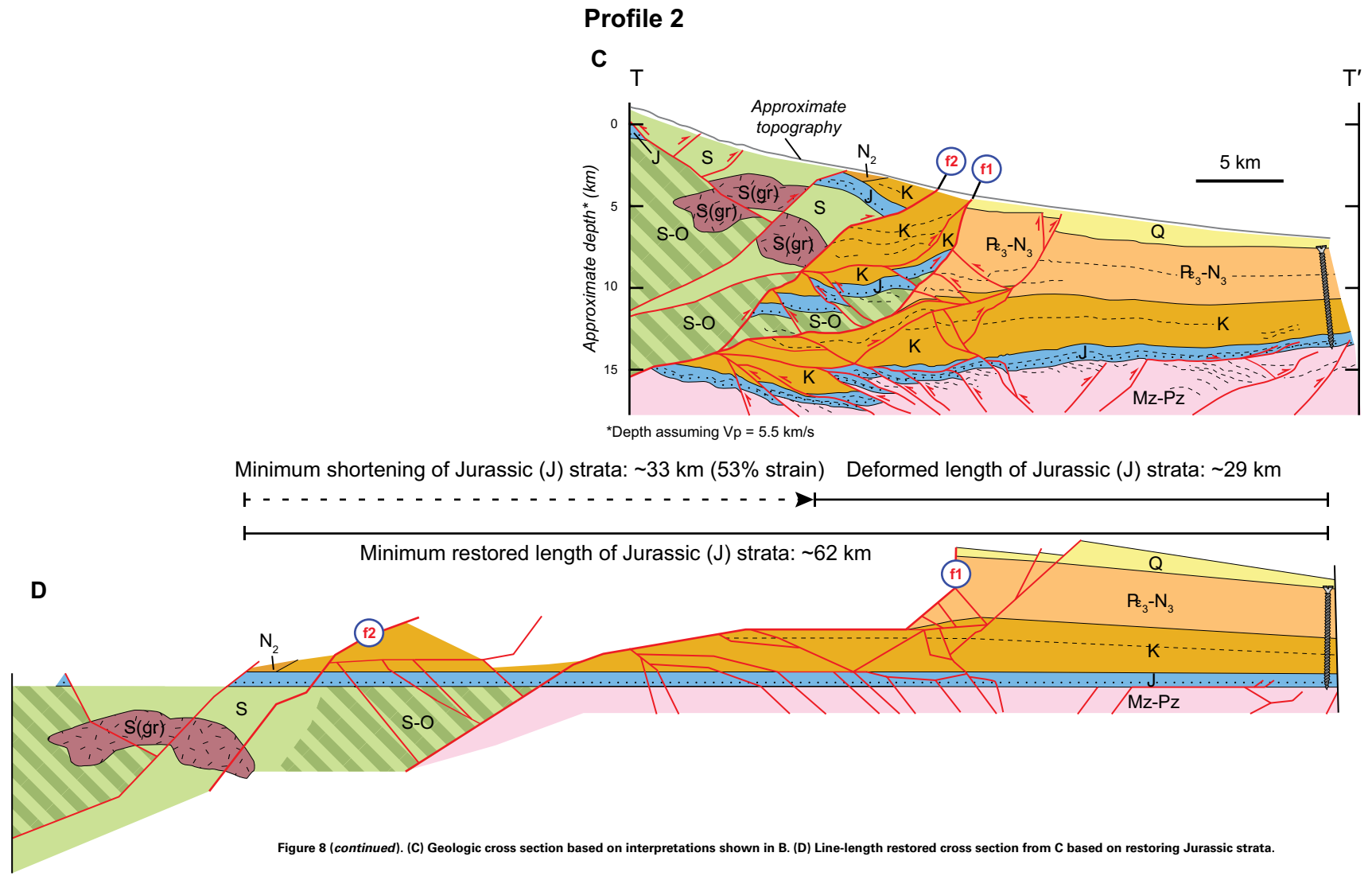

Figure 8 (*continued*). (C) Geologic cross section based on interpretations shown in B. (D) Line-length restored cross section from C based on restoring Jurassic strata.

Geosphere, published online on 5 February 2016 as doi:10.1130/GES01254.1

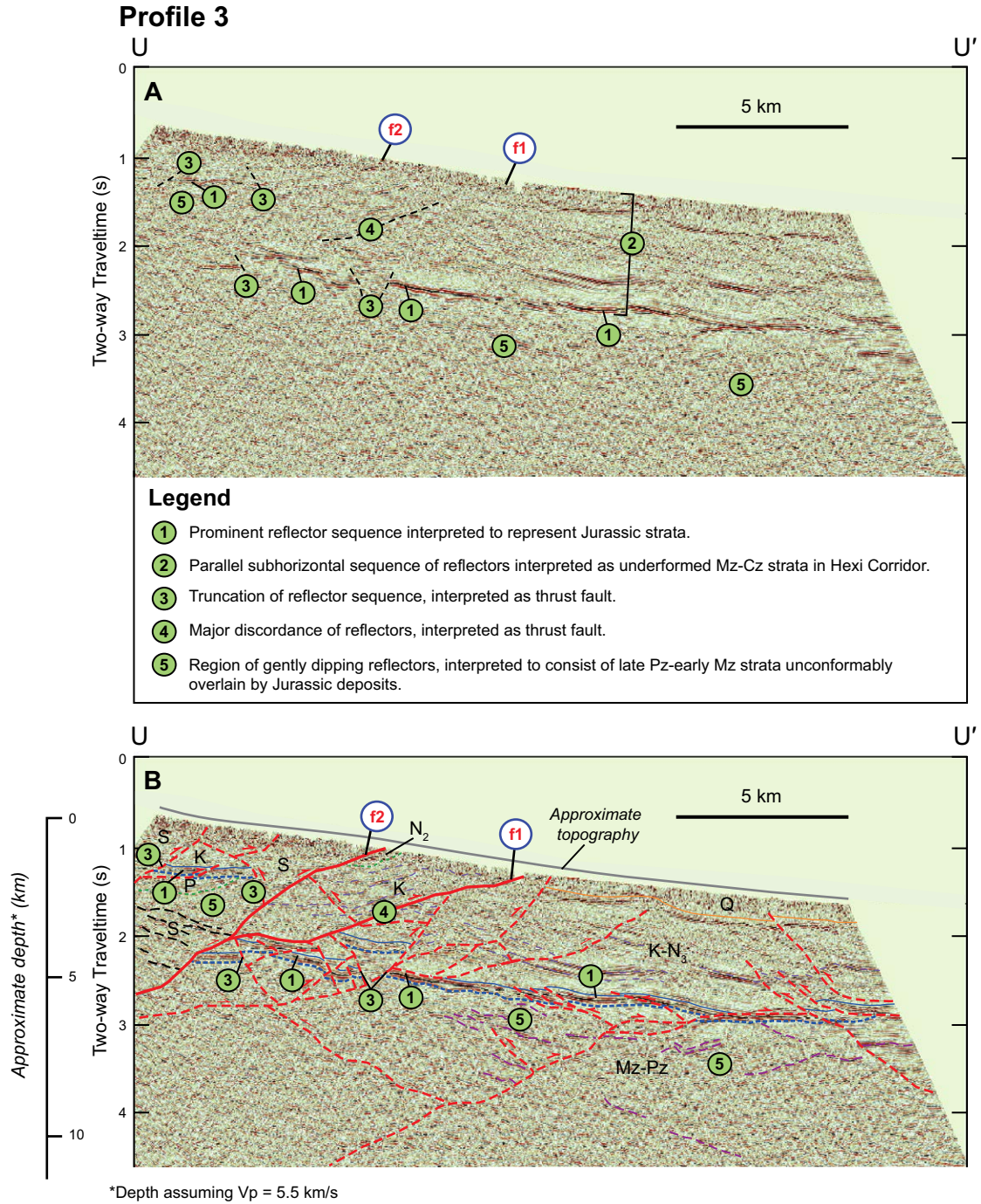

Figure 9 (*on this and following page*). (A) Uninterpreted seismic reflection profile (high-resolution uninterpreted seismic reflection profile can be found in the in Supplemental File 1. See Figures 1, 3, and 5 for location. Key features, including prominent reflectors and truncations, are labeled from 1 to 5 and described in the legend. (B) Interpreted seismic reflection profile. Important features are labeled as in A.

Geosphere, published online on 5 February 2016 as doi:10.1130/GES01254.1

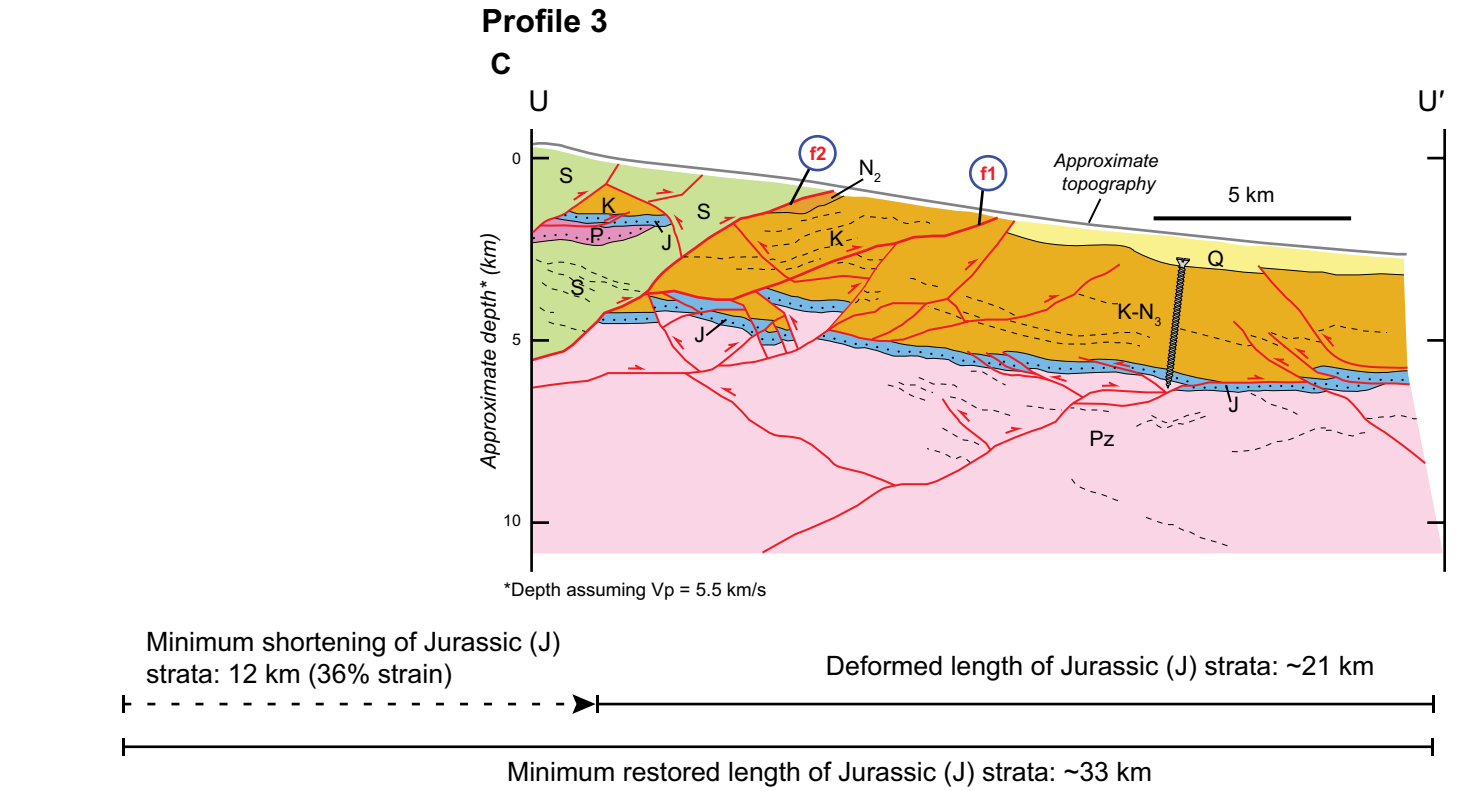

Figure 9 (*continued*). (C) Geologic cross section based on interpretations shown in B. (D) Line-length restored cross section from C based on the restoration of Jurassic strata. See Figure 5 for abbreviations. Pz—Paleozoic.

Geosphere, published online on 5 February 2016 as doi:10.1130/GES01254.1

Jurassic strata are interpreted to overlie Carboniferous–Triassic rocks with a minor (10°–15°) angular unconformity (between labels 1 and 6 in Fig. 7), although the distinct units beneath the Jurassic strata are not constrained. The coherent layer of Jurassic strata pinches out in the south end of the profile (Fig. 7). This interpretation is further supported by the lack of Jurassic rocks exposed at the surface to the south-southwest of this profile location (Fig. 5). The relatively transparent Silurian granitoid and Ordovician–Silurian metasedimentary rock compose most of the southern portion of the acquired image (label 5 in Fig. 7). The truncation of poorly organized, tightly folded, and diffuse reflectors represents an intrusive contact of granitoid against Ordovician–Silurian metasedimentary rocks.

This profile images two major thrust faults (Figs. 5 and 6). The most northern structure (f1 in Fig. 7) involves a nearly continuous and parallel set of south-dipping (25°–35°S) reflectors juxtaposed against horizontal reflectors near the middle of the image (3 and 4 in Fig. 7). We interpret this structure as a hanging-wall flat–footwall ramp thrust fault. Hanging-wall rocks are interpreted to be Cretaceous in age based on projecting surface geology to depth (Figs. 5 and 7). The Jurassic strata pinch-out could alternatively be interpreted as a footwall ramp truncation, which would require a matching Jurassic cutoff in the hanging wall. We do not prefer this interpretation because this relationship is not observed. Slip along f1 is at least 15–20 km. The second major fault (f2 in Fig. 7) truncates the Cretaceous hanging-wall strata of fault f1 and places the relatively transparent Ordovician–Silurian units against the Cretaceous rocks (Fig. 7). Based on the observed fault geometries and unit juxtapositions, slip along this second fault, f2, is likely 5–10 km. Some of the observed unconformities (i.e., beneath the Jurassic strata) could be low-angle hanging-wall bedding-parallel thrusts, but we prefer the unconformity interpretation based on the regional geology and because this assumption minimizes estimated shortening.

Seismic reflection profile 2 (Fig. 8) (line T–T′ in Fig. 5) is an ~39-km-long section located ~40 km to the southeast of profile 1 (Fig. 5). This section images the same south-dipping thrust structures and undeformed foreland observed in profile 1. Strongly reflective Jurassic strata are ~8 km below the surface of the Hexi Corridor (1 in Fig. 8) and are overlain by Cretaceous–Quaternary sedimentary rocks (2 in Fig. 8). Middle Miocene rocks at the base of the range (N in Fig. 5) are syntectonic because they unconformably overlie Cretaceous strata and are truncated by the current range-bounding thrust (Fig. 8). This supports middle Miocene fault initiation. Jurassic strata overlie Triassic or Paleozoic rocks with an apparent angular unconformity of ~15° (between 1 and 6 in Fig. 8), similar to profile 1 (Fig. 7). Minor south-dipping faults disrupt Paleozoic through Jurassic strata in the north.

The southwestern side of the seismic profile shows also shows two major faults. The first brings Jurassic strata from a depth of ~8 km to ~5 km along a thrust fault (f1 in Fig. 8). This juxtaposition, along with the observed fault geometry, requires a minimum fault slip of ~15 km. The hanging-wall rocks in f1 are truncated by another major fault (f2 in Fig. 8) that brings Ordovician–Silurian and Jurassic strata over Jurassic–Cretaceous rocks (3 in Fig. 8), which requires ~10–15 km of slip. Another minor south-dipping fault transports early Paleozoic rocks and truncates north-dipping Jurassic strata. Slip on this fault is poorly constrained but must be large enough (2–4 km) to expose Silurian rocks in this range (Fig. 5) and to cut through and obscure Jurassic strata at the surface (Fig. 8).

Seismic reflection profile 3 (Fig. 9) (line U–U′ in Fig. 5) is an ~25 km-long section located ~10 km to the southeast of profile 2 (Fig. 5). This is the only section that is parallel and aligned with shortening in the Yumu Shan to the northeast (Figs. 1 and 10), and the imaged structures may be kinematically linked with those to the north (Tapponnier et al., 1990). The prominent reflector sequence that is interpreted to represent Jurassic strata is located at a depth of 3–4 km below the Hexi Corridor (label 1 in Fig. 9), compared to depths of 6–8 km in the other two profiles (Figs. 7 and 8). Thus, Cretaceous–Cenozoic deposits in this section are 2–4 km thinner than the other sections, although the relative thickness of each different-aged deposit is ambiguous (e.g., Cretaceous versus Neogene versus Quaternary strata). This thickness difference may be caused by either a Cretaceous or Cenozoic paleohigh that impeded the deposition of Cretaceous or Cenozoic sediments, or earlier localized Cenozoic uplift that allowed for more erosion of the youngest sedimentary rocks. Jurassic strata overlie Triassic or Paleozoic rocks with an angular unconformity of ~10° (between labels 1 and 5 in Fig. 9).

Unlike the other profiles, at least five north-dipping faults cut through Hexi Corridor sedimentary rocks with small-magnitude offsets. These south-directed faults may originate from deformation in the Yumu Shan (Figs. 1

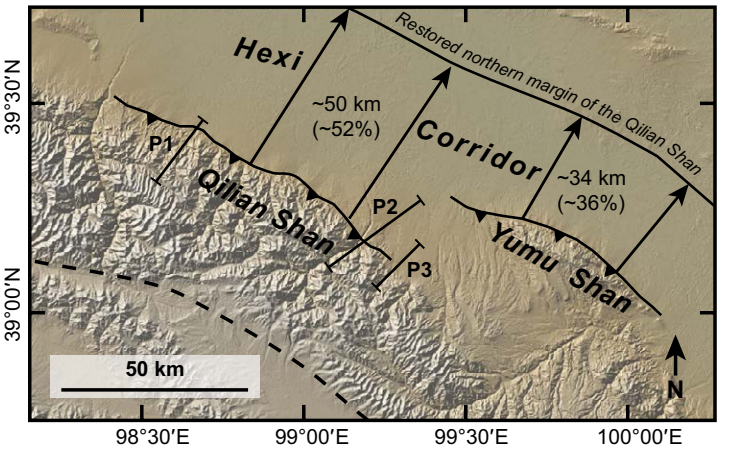

Figure 10. Sketch map showing reconstruction of the pre-Cenozoic northern margin of the frontal Qilian Shan relative to the present-day based on the shortening estimates obtained in this study. This map highlights the fact that lower magnitude shortening in the east are balanced by an overall wider zone of deformation, as strain is also occurring in the Yumu Shan. P1, P2, and P3 refer to profiles 1, 2, and 3, respectively. Note that P3 is in line with the Yumu Shan thrust system whereas the other seismic profiles are not.

Geosphere, published online on 5 February 2016 as doi:10.1130/GES01254.1

and 10). Two major thrusts are imaged in the southern portion of this profile. The first thrust (f1 in Fig. 9) creates the geometric relationship of south-dipping Cretaceous strata in the hanging wall against nearly horizontal strata in the footwall, near the middle of the section (4 in Fig. 9). This juxtaposition requires a minimum ~3–5 km of slip. The second major thrust (f2 in Fig. 9) is imaged at the southern edge of profile 3 and involves the movement of Jurassic–Cretaceous rocks to within 1–2 km of the surface along a south-dipping fault. A backthrust in the hanging wall truncates Jurassic strata, and only Silurian rocks are exposed at the surface along the profile surface trace (Fig. 5). Jurassic beds are exposed south of profile 3 (Fig. 5).

Cross-Section Models and Cenozoic Shortening Estimates

Given that contractional deformation of Carboniferous and younger beds is interpreted to be Cenozoic in age, the restoration of our balanced cross sections provides constraints on the minimum magnitude of Cenozoic shortening strain. The following assumptions went into balanced cross-section construction and restoration. (1) When hanging-wall cutoffs are eroded, minimum fault offsets were used in the restorations. (2) Deformation is plane strain in the north-northeast–trending sections; this is validated by direct field observations of dip-slip fault kinematics (e.g., fault slickenlines and asymmetric minor folding analysis; Reith, 2013; our field observations), present-day north-northeast–south-southwest convergence as indicated by GPS velocities, and a northeast contractional strain field (Zhang et al., 2004; Allmendinger et al., 2007). (3) The unconformity at the base of the Jurassic strata has no initial relief and is restored to horizontal. The contact between Jurassic and Triassic strata, where it is directly observed in the field, is parallel to subparallel (~<15° discordance) and was likely initially horizontal. (4) The pin lines are placed in the relatively undeformed footwall of the Hexi Corridor foreland, pinning Jurassic–Quaternary strata. (5) Shortening estimates are a minimum because of hanging-wall erosion (Boyer and Elliott, 1982), bed-length changes during deformation (Groshong et al., 2012), cleavage formation, unrecognized additional detachment surfaces at depth (e.g., Yin et al., 2008a), and unconstrained deformation in the early Paleozoic granite and metasediments. (6) Although significant pre-Cenozoic deformation affected the region, following the logic presented here, restoration of Jurassic–Cretaceous strata provides an estimate of Cenozoic strain. (7) The use of a single average seismic velocity leads to horizontal length errors of <4%. The balanced and restored cross sections are presented in Figures 7–9.

Because the Jurassic strata in seismic reflection profile 1 (Fig. 7) are not observed in the hanging wall, either because it pinches out or is truncated by a fault, and the Cretaceous hanging-wall cutoff is also eroded, line-length balancing of either of these units would lead to large uncertainties. An alternative method is required to constrain shortening. Profile 1 is located within 2 km of the parallel traverse by Zheng et al. (2010) (Fig. 5), allowing us to use their AHe data in our deformed and restored cross-section models. Their study locates a ca. 10 Ma apatite paleo-PRZ in the hanging wall of the north-directed thrust system (e.g., Fig. 4C), which can be used to estimate the location of a ca. 10 Ma paleoland surface at ~2.6 km above the paleo-PRZ, assuming a typical continental geothermal gradient and reasonable AHe closure temperature (see discussion in Zheng et al., 2010). We place this paleo-PRZ and ca. 10 Ma paleoland surface in our deformed-state cross section (Figs. 7B, 7C) and use it in our restoration to align this ca. 10 Ma marker horizon (i.e., the paleoland surface) within middle Miocene strata in the Hexi Corridor footwall (Fig. 7D). The same method was used by Zheng et al. (2010), but with only one fault strand and an oversimplified fault geometry. Our seismic interpretation and knowledge of the fault geometries at depth allows for a better constrained restoration. We restore the paleo-PRZ within the Silurian granitoid along the imaged thrust faults until the inferred ca. 10 Ma paleoland surface is at the same vertical position as the ca. 10 Ma strata in the footwall (Fig. 7D). This restoration requires a good vertical scale to be meaningful, but the vertical scale of our seismic sections is only an approximation. To overcome this issue, we use three independent observations to verify the vertical position. First, we compare the relative scale of our cross-section model with that presented by Zheng et al. (2010) that shows that the paleo-PRZ in the hanging wall is located ~2.1 km above the ca. 10 Ma surface in the Hexi Corridor. Our cross-section model shows a similar vertical relationship. Second, Cretaceous beds are ~3 km thick (see preceding discussion) and we can compare the apparent thickness of these beds in the seismic section to create a local vertical scale. Third, we note that the Carboniferous strata unconformably overlying the Silurian pluton (Figs. 5, 7B, and 7C) must be restored to a viable pre-Cenozoic position to avoid creating an unreasonable buttress unconformity, which would indicate large-scale relief during the deposition of Cretaceous strata.

We position the Silurian pluton to minimize shortening (Fig. 7D), although allowing more slip would give the implied unconformities a more realistic geometry with less pre-Cenozoic relief. To the south of the Silurian pluton, the lack of bedded units and coherent reflectors makes restoration difficult. Silurian and Ordovician strata are involved in imbricate thrusting that may be either Paleozoic or Cenozoic in age (Figs. 5 and 7). With our restoration method, we calculate a minimum horizontal shortening magnitude of 25 km with a deformed section length of 21 km, which yields a minimum shortening strain of 54% (Fig. 7D). Alternatively, if we ignore the AHe data and retrodeform the strata along the observed footwall fault geometries, minimum shortening is 22 km (53% strain). The latter method does not adequately restore the Carboniferous unconformity to a reasonable elevation, so we prefer the former shortening estimate (i.e., 25 km or 54% strain). A line-length balance of Cretaceous strata yields a shortening magnitude of 15 km and a corresponding strain of 40%, which can be regarded as absolute minimum estimates. If the strain was accommodated over the past ~10 m.y. (Zheng et al., 2010), the corresponding horizontal shortening rate and strain rate are 2.2–2.5 mm yr^{-1} and 1.7×10^{-15} s^{-1}, respectively.

Profile 2 (Fig. 8) is retrodeformed to an undeformed pre-Cenozoic state by restoring the Jurassic beds (i.e., the prominent reflectors labeled 1; Figs. 8A, 8B) to a continuous and horizontal position (Fig. 8D). The minimum magni-

Geosphere, published online on 5 February 2016 as doi:10.1130/GES01254.1

tude of horizontal shortening calculated by this restoration is ~33 km across a deformed section length of ~29 km (Fig. 8D), which yields a shortening strain of 53%. The surface exposure of Jurassic strata in the hanging wall in the Qilian Shan range (Fig. 5) and the reasonably constrained location of Jurassic rocks in the Hexi Corridor footwall (Fig. 8) require a minimum vertical throw of 8–10 km. This observation corroborates our interpretation and requires shortening of this approximate magnitude. Given that this strain was accommodated since ca. 10 Ma (Zheng et al., 2010), the corresponding horizontal shortening rate and strain rate are 3.3 mm yr^{-1} and 1.7×10^{-15} s^{-1}, respectively.

Seismic reflection profile 3 (Fig. 9) is also restored using the Jurassic unit as a marker horizon (i.e., the prominent sequence of reflectors labeled 1 in Fig. 9). Motion on fault f2 is poorly constrained because of erosion of the hanging-wall cutoff, but there must be enough slip on fault f2 to expose Silurian strata at the surface (e.g., Fig. 5). The minimum magnitude of horizontal shortening calculated in this restoration is ~12 km across a deformed section with a length of 21 km, yielding a minimum strain of 36%. Assuming that deformation initiated ca. 10 Ma (Zheng et al., 2010), the corresponding horizontal shortening rate and strain rate are 1.2 mm yr^{-1} and 1.1×10^{-15} s^{-1}, respectively.

DISCUSSION

Cenozoic Shortening across the Northeastern Tibetan Plateau

Our analysis of seismic reflection profiles yields minimum north-south shortening estimates of 25 km (54% strain), 33 km (53% strain), and 12 km (36% strain), from west to east (Figs. 3 and 5). Although our seismic reflection interpretations, cross-section models, and section restorations are nonunique solutions, the geometric compatibility between the three sections adds robustness to our interpretations. All three profiles image two south-dipping strands of the northern Qilian Shan frontal thrust system. In all three cross sections, Quaternary sediments cover fault 1, and fault 2 represents the range-bounding fault (Fig. 5), suggesting that fault 1 is inactive and fault 2 is active. This trailing imbricate system may have first exploited the relative weaknesses within the bedded Cretaceous rocks before cutting through early Paleozoic strata.

Profiles 1 and 2 yield similar shortening magnitude and strain estimates. One explanation for profile 3 having a lesser magnitude of Cenozoic shortening is that deformation may be partitioned between the Qilian Shan and Yumu Shan thrust systems, ~25 km northeast of profile 3 (e.g., Tapponnier et al., 1990) (Fig. 10). Profile 3 is the only section that is directly in line with the Yumu Shan. Estimated north-south shortening rates across the Yumu Shan are 0.4–1.9 mm yr^{-1} (Tapponnier et al., 1990) and if faulting also initiated ca. 10 Ma, the magnitude of shortening should be between 4 and 19 km. Summation of the shortening magnitudes and rates from the Yumu Shan and the Qilian Shan frontal thrust system imaged in profile 3 yields 16–31 km (33%–49% strain) and 1.6–3.1 mm yr^{-1}, respectively, consistent with the shortening observed in profiles 1 and 2 to the west (Fig. 10).

Shortening estimates derived from the longest profile (i.e., profile 2; Fig. 8) indicate that the northern Qilian Shan minimum Cenozoic shortening magnitude and strain were 33 ± 6 km and 52% ± 4%, respectively, including the uncertainties associated with using a single uniform seismic velocity. Other seismic reflection analyses across the northern Qilian Shan frontal thrust system obtain comparable strain values of 40%–55% (J. Wu et al., 2006; Yang et al., 2007a, 2007b). Assuming that this strain can be applied across the width of the northern Qilian Shan frontal range (40–50 km), a possible restored position of the northern margin of the Qilian Shan prior to Cenozoic shortening is shown in Figure 10. Note that all three profiles restore to a similar position.

The north-south shortening rate across the northern Qilian Shan thrust system derived from this study, 3.3 ± 0.6 mm yr^{-1}, is much higher than most other rate estimates across northern Tibet (Hetzel et al., 2004; W.J. Zheng et al., 2009, 2013; D. Zheng et al., 2010; Yuan et al., 2011), but is consistent with the estimates of Champagnac et al. (2010) (i.e., ~2.5 mm yr^{-1}), also along the northern Qilian Shan. If correct, these high deformation rates indicate that deformation is currently focused along the northern margin of the plateau, and that the northern Qilian Shan thrust faults accommodate more than half of the entire geodetic shortening across the Qilian Shan–Nan Shan thrust belt (i.e., ~5.5 mm yr^{-1}) (Zhang et al., 2004).

The Cenozoic shortening documented in this study is also higher than other estimates around the northeastern Tibetan Plateau (Fig. 3). This disparity may be due to either a heterogeneous strain distribution in northern Tibet or an artifact of the limitations of strain estimates that are calculated from observations of the surface geology alone. Estimates derived from restoring only Cenozoic strata are significantly lower (<15% strain) (e.g., Lease et al., 2012; Craddock et al., 2014) than those that incorporate subsurface data (>40% strain) (J. Wu et al., 2006; Yang et al., 2007a, 2007b; Yin et al., 2008b; Gao et al., 2013; this study). However, the variable topography, eastward-tapering thrust belts (Fig. 1), complex interaction between strike-slip and thrust faulting, and heterogeneous strain estimates in different cross sections from the same study (e.g., Fig. 3) suggest that strain is not spatially constant across northern Tibet. By integrating our calculations with other seismic analyses and regional bulk shortening estimates (e.g., Yin et al., 2008b; Meyer et al., 1998; Gao et al., 2013), we suggest that the bulk Cenozoic strain across the Qilian Shan–Nan Shan thrust system is >30% (215–300 km shortening) (Fig. 3; Table 2); higher strain (>53% or ~50 km shortening) is concentrated in the northern Qilian Shan thrust belt along the plateau margin. Thus, the higher strain observed along the northern Qilian Shan should not be extrapolated across the entire Qilian Shan–Nan Shan thrust belt.

Our analysis suggests that a significant portion of the convergence between North China and Tibet (~5.5 mm yr^{-1}) is accommodated by concentrated shortening across the northern Qilian Shan frontal thrust system (3.3 ± 0.6 mm yr^{-1}). This result indicates that focused deformation along the northern margin of the Tibetan Plateau is similar to Himalayan shortening along the southern margin of the plateau, where strain is highly concentrated along the Main Frontal Thrust (Lavé and Avouac, 2000; Burgess et al., 2012).

Geosphere, published online on 5 February 2016 as doi:10.1130/GES01254.1

Crustal Shortening, Thickening, and Denudation

To quantitatively evaluate plateau formation mechanisms, we first determine the significance of distributed shortening in crustal thickening and plateau development. A well-constrained estimate of the pre-Cenozoic crustal thickness of northern Tibet is required to assess the role that crustal shortening has in crustal thickening. Although such an estimate does not exist, several lines of evidence suggest that the pre-Cenozoic thickness of the northern Tibet was ~40 km. The global average thickness of modern continental crust is 41 ± 6 km (Christensen and Mooney, 1995). Although Mesozoic rifting is widespread across northern Tibet (Vincent and Allen, 1999; Chen et al., 2003) and rifted crust can be as thin as 36 ± 8 km (Christensen and Mooney, 1995), nonmarine Cretaceous deposits require the crust to be at least 32–34 km thick to be above sea level, given Airy isostatic compensation (e.g., Schubert and Sandwell, 1989). Furthermore, the Ordos Basin to the northeast of the plateau (Fig. 1) represents relatively stable crust, with a lack of earthquakes and a lower average elevation (i.e., ~1.3 km). Its current crustal thickness of ~42 km (Liu et al., 2006) is a good approximation for crustal thickness in the adjacent northern Tibet prior to Cenozoic deformation.

The horizontal crustal shortening observed across northern Tibet (Table 2) contributes to crustal thickening of this initially ~40-km-thick crust, assuming that surface and mantle erosional processes and/or lateral material transport (i.e., not plane strain shortening) are not outpacing crustal thickening. Vertical thickening results from horizontal shortening assuming the following: (1) vertically uniform horizontal plane strain shortening of the crust (i.e., upper, middle, and lower crust), (2) two-dimensional (2-D) pure shear crustal thickening, and (3) minor, or at least well-constrained, denudation. Horizontal shortening strain, ε_h, is defined as $\varepsilon_h = \frac{l_f - l_i}{l_i}$, where l_f and l_i are the final and initial cross-section lengths, respectively. Horizontal shortening strain can be converted to horizontal stretch strain, $s_h = \frac{l_f}{l_i} = \varepsilon_h + 1$, which is inversely related to the vertical stretch strain, $s_v = \frac{1}{s_h}$. The apparent present-day crustal thickness, T_f, relates to vertical stretch strain (s_v) as $T_f = T_i \times s_v$, where T_i is the initial crustal thickness. This same approach can be used to back-calculate the apparent predeformational crustal thickness of the Tibetan Plateau (Table 2).

This simple approximation excludes the effects of denudation; however, we have determined <5 km of Cenozoic denudation across northern Tibet. The Silurian–Carboniferous unconformity in the hanging wall of the Qilian Shan frontal thrust system (Figs. 5 and 7) constrains how much material was removed to expose this marker horizon. Carboniferous–Jurassic strata are ~4–4.5 km thick and Jurassic–Cretaceous rocks record a transition from marginal marine to nonmarine deposits (Gansu Geological Bureau, 1989; Qinghai BGMR, 1991). The exposure of the base Carboniferous beds (i.e., the unconformity surface) requires 4–4.5 km denudation since the beginning of the Cretaceous, when terrestrial sedimentation began (Vincent and Allen, 1999) and erosion could have commenced. The magnitude of Cretaceous versus Cenozoic erosion and/or denudation is not constrained, and so this estimate provides a maximum Cenozoic denudation magnitude of 4.5 km. The AHe study of Zheng et al. (2010) shows erosion and denudation magnitudes of ~2 km since ca. 10 Ma. We assume a conservative maximum denudation magnitude of 5 km across the northern Qilian Shan thrust system and assume that all of northern Tibet underwent a similar magnitude of denudation.

Assuming that the crustal thickness of northern Tibet prior to India-Asia collisions is ~40 km, we calculate the crustal thickness that develops due to horizontal shortening (Table 2), and compare this value to the present-day crustal thickness (55–65 km) (e.g., Fig. 1C) of northern Tibet (Fig. 11). When crustal shortening alone generates a crustal thickness that agrees with modern observations, no additional mechanisms are favored for plateau development, but if the shortening estimates overthicken or underthicken the crust, alternative processes, including channel flow or underthrusting (e.g., Fig. 2), are required. We conduct this analysis on two northeast-trending cross-section lines across northern Tibet (lines J–J′ and K–K′ in Fig. 3) (Fig. 11).

In the west, along line J–J′ in Figure 3, the observed crustal shortening estimates in the Qimen Tagh, Qaidam Basin, and Qilian Shan–Nan Shan thrust belts can effectively explain the present-day crustal thickness (Fig. 11). The shortening observed in our seismic profiles at the northern edge of the Qilian Shan is high and predicts thicker crust (i.e., 75–80 km) than what is observed. In the east, along line K–K′ in Figure 3, shortening estimates south of the Haiyuan fault near the Gonghe Basin (Fig. 3) are too low to adequately explain the observed crustal thickness (Fig. 11); an extra crustal thickness of ~10 km is needed. To the north of the Haiyuan fault crustal shortening is sufficient to develop the observed ~50-km-thick crust (Fig. 11). The higher shortening reported by Gao et al. (2013) predicts thicker crust than what is observed (~70–75 km) (Fig. 11).

This integrated analysis can ascertain the importance of distributed shortening as a plateau formation mechanism. For most of northern Tibet, away from the plateau margins, distributed crustal shortening and pure shear thickening can adequately generate the observed 55–65 km crustal thickness (Fig. 11), which suggests that distributed shortening is the dominant crustal thickening process operating through most of this region. The higher strain observed by our seismic reflection analysis along the plateau margin may result from either southward underthrusting of the Asian mantle lithosphere or continental subduction (Table 1). Given that this higher magnitude deformation is focused along the northern margin of the plateau and not along existing sutures (Fig. 1), the underthrusting model is favored. If the Asian mantle lithosphere is underthrust to a position near Qaidam Basin, as suggested by Ye et al. (2015) (Fig. 1A), ~300 km shortening (~50%) is required to accommodate this motion.

Coherent Model for the Cenozoic Development of the Northeastern Tibetan Plateau

We integrate existing work across northern Tibet to develop a lithospheric-scale model for the Cenozoic development of the northeastern Tibetan Plateau (Fig. 12). We suggest that the crustal thickness and eleva-

Geosphere, published online on 5 February 2016 as doi:10.1130/GES01254.1

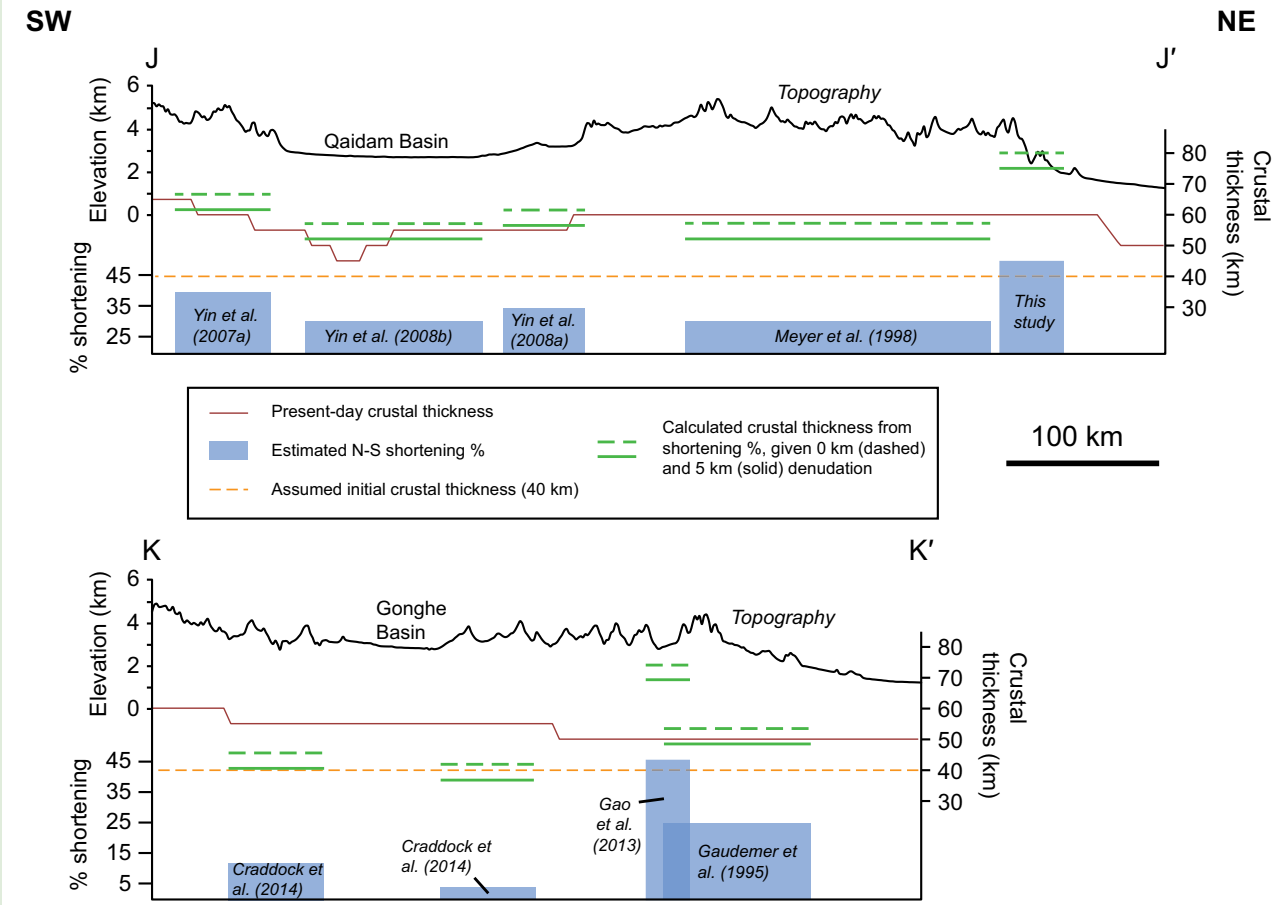

Figure 11. Comparison plot of topography (black lines), crustal thickness (red lines), estimated percent crustal shortening (blue boxes), and predicted present-day crustal thickness (dashed green line = no denudation; solid green line = 5 km denudation) given pure shear thickening at estimated shortening strain magnitude along the segment assuming an initial crustal thickness of 40 km (dashed orange line). Section lines J–J′ and K–K′ are shown in Figure 3. Crustal thickness values are from Yue et al. (2012) (Fig. 1C) and shortening estimates discussed in text. Note that when crustal shortening and pure shear thickening cannot account for the observed present-day crustal thickness, an alternative plateau formation mechanism is favored.

tion of the northeastern Tibetan Plateau are the results of bulk north-south shortening of the Tibetan-Asian lithosphere by at least 250–350 km, from the Kunlun fault in the south to the Hexi Corridor in the north (Figs. 1 and 12). This shortening is accommodated by southward underthrusting of the Asian mantle lithosphere beneath the northern margin of the plateau and a similar magnitude of crustal shortening and pure shear crustal thickening (Fig. 12). Strain observed away from the margins of the northeastern plateau is ~30%–45%, which is sufficient to thicken an initially ~40-km-thick crust to the present-day crustal thickness solely by distributed crustal shortening and pure shear thickening. With this scenario, the Tibetan crust has thickened by ~20 km via distributed contractional folding and faulting as a result of deformation that transferred rapidly from the south, as early as ca. 50 Ma (Yin et al., 2008a; Duvall et al., 2013). Localized higher strain (>53%) along the northern plateau margin results from southward underthrusting of the Asian mantle lithosphere to a position beneath northern Qaidam Basin. This is supported by receiver function studies that image the south-dipping North China mantle lithosphere beneath the Tibetan Plateau (Feng et al., 2014; Ye et al., 2015). However, our observations are not consistent with the high of magnitude of underthrusting envisioned by Kind et al. (2002) (Fig. 1A) that would require significantly more upper crustal shortening (Fig. 2D). The relatively recent initiation of faulting (Zheng et al., 2010) and high strain rates (Champagnac et al., 2010; this study) along the northern plateau margin suggest that this interpreted underthrusting is a young feature of plateau development that initiated at around 10 Ma.

Geosphere, published online on 5 February 2016 as doi:10.1130/GES01254.1

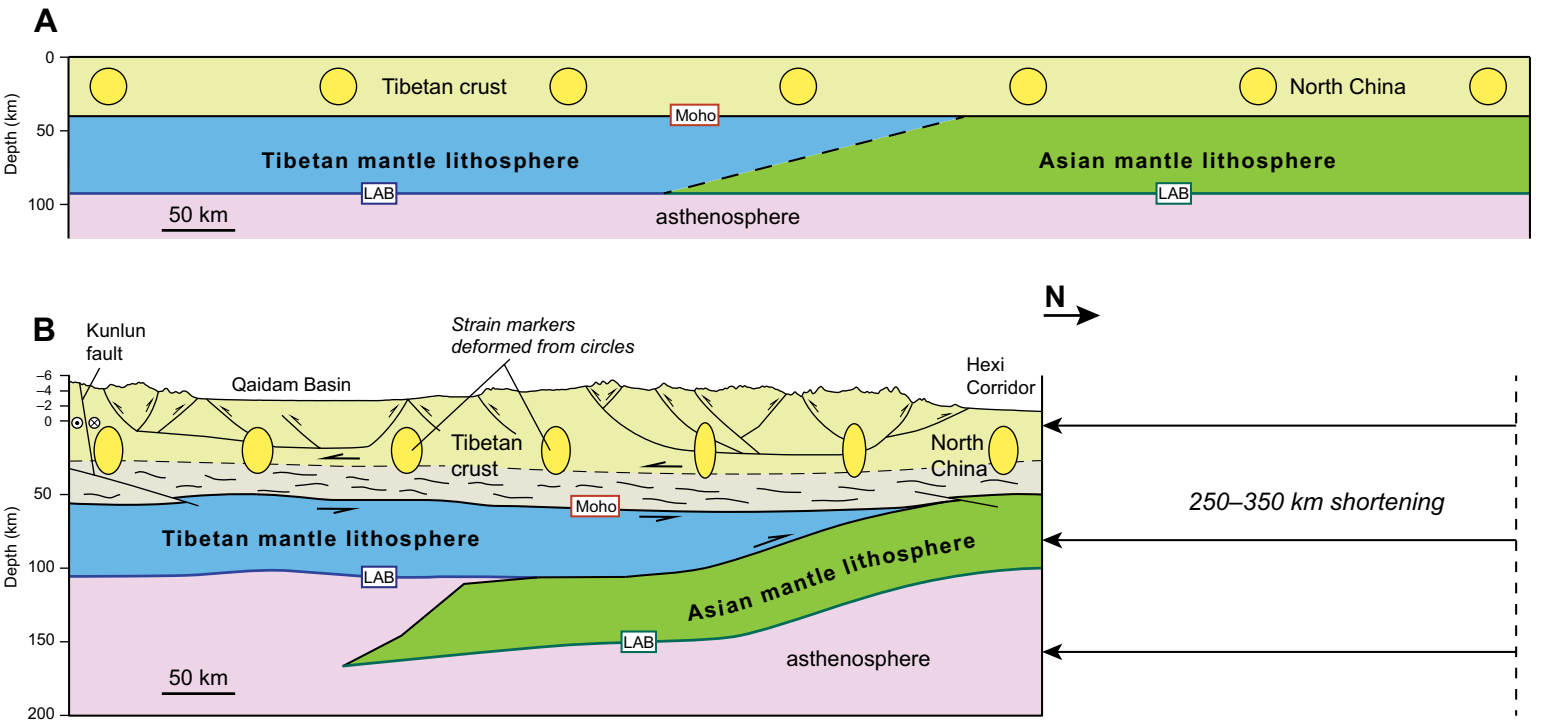

Figure 12. Our preferred lithospheric-scale model for the development of the northeastern Tibetan Plateau, between the Kunlun fault in the south and the Hexi Corridor in the north. (A) The pre-Cenozoic undeformed Tibetan and Asian continental lithosphere. (B) 250–350 km of Cenozoic convergence between Qaidam Basin and North China is accommodated by southward underthrusting of the Asian mantle lithosphere beneath Tibet and distributed vertically—uniform crustal shortening. The strain ellipses deformed from circles illustrate the relative magnitude of contractional strain along this profile. Note that with the exception of the top 6 km, there is no vertical exaggeration in this profile. Crustal structures, including subhorizontal shear zones, Moho depth, and lithosphere-asthenosphere boundary (LAB) positions are from Gao et al. (1999, 2013), Wang et al. (2011), Feng et al. (2014), and Ye et al. (2015).

Although most of the observed strain distribution (Fig. 3) can be explained by our lithospheric-scale model (Fig. 12), the low shortening magnitudes (<15%) near the Gonghe Basin and the Jishi-Laji Shan to the southeast require explanation (Lease et al., 2012; Craddock et al., 2014). These relatively low shortening estimates may be the result of shortening underestimation because of the lack of subsurface data, although Lease et al. (2012) argued that these low shortening magnitudes are sufficient to generate the observed crustal thickness from crust with an initial thickness of 45 ± 5 km. Alternatively, these low strain magnitudes may indicate that a different mechanism is operating in this eastern region of northern Tibet (Fig. 1B), such as northeast-east–directed lower crustal flow around Sichuan Basin (Clark and Royden, 2000) that could lead to additional vertical crustal thickening without horizontal crustal strain at the surface. The lateral flow of low-viscosity material may be driven by the northward indentation of India into the Tibetan lithosphere from the south or the southward underthrusting of the Asian mantle lithosphere beneath northern Tibet.

Accommodation Mechanisms of India-Asia Convergence

There has been 2000–2500 km of convergence between India and Asia since the onset of collision at 65–55 Ma (e.g., Molnar and Tapponnier, 1975; Dewey et al., 1989; Le Pichon et al., 1992; Zhu et al., 2005; van Hinsbergen et al., 2011). Efforts to document this convergence in crustal shortening generally come up short, with 600–900 km shortening in the Himalaya (DeCelles et al., 2002; Robinson et al., 2006; Yin et al., 2010b; Long et al., 2011; Webb, 2013) and 300–400 km of north-south shortening reported across all of Tibet (e.g., Yakovlev and Clark, 2014). These low values for Tibetan shortening need to be reconsidered in light of detailed field and seismic subsurface data. By integrating our results across the northern Qilian Shan thrust system with other robust estimates discussed in this paper (e.g., Gaudemer et al., 1995; Meyer et al., 1998; Yin et al., 2008a, 2008b; Reith, 2013; Gao et al., 2013), we suggest that the entire 350-km-wide Qilian Shan–Nan Shan thrust belt accommodates a

Geosphere, published online on 5 February 2016 as doi:10.1130/GES01254.1

minimum of 215–300 km Cenozoic shortening. Higher strain of >53% is occurring along the northern plateau margin, whereas lower strain of 30%–45% is occurring within the thrust belt interior (Table 2). Given that similar strain magnitudes have been documented in the Qimen Tagh, Qaidam Basin, and North Qaidam thrust belts (Yin and Harrison, 2000; Yin et al., 2007a, 2008a, 2008b; Wang et al., 2011) (Figs. 1 and 3; Table 2), at least 250–350 km of north-south Cenozoic shortening may have been absorbed between Hexi Corridor and the Kunlun fault (Figs. 1 and 12). These extrapolations require further testing, but demonstrate that crustal shortening and the construction of the northeastern Tibetan Plateau play a significant role in accommodating the >2000 km convergence between India and Asia.

CONCLUSIONS

The following conclusions can be drawn from the integration of our seismic reflection analysis with other existing structural studies across northern Tibet.

1. Many satellite- and field-based Cenozoic shortening estimates across the Qilian Shan–Nan Shan thrust belt are low (e.g., <15%–20%). We posit that these studies underestimate crustal strain across northern Tibet by missing blind structures and detachments. More robust studies, including other seismic reflection analyses and regional bulk shortening estimates, suggest that strain across most of northern Tibet, from the Qimen Tagh in the south to the Qilian Shan in the north, is >30%–45%.

2. Our seismic reflection analysis across the northern Qilian Shan reveals a south-dipping Cenozoic thrust system that places Paleozoic and Mesozoic strata on undeformed Mesozoic–Cenozoic sediments in the Hexi Corridor foreland. Our upper crustal north-south shortening estimates are 25 km (54% strain), 33 km (53% strain), and 12 km (36% strain). The lowest shortening estimate is likely due to deformation being partitioned between the Qilian Shan and the Yumu Shan thrusts. We prefer the values from our longest seismic reflection profile and suggest that the northern Qilian Shan accommodates a minimum crustal shortening strain, shortening rate, and strain rate of ~53%, 3.3 ± 0.6 mm yr^{-1}, 1.7 × 10^{-15} s^{-1}, respectively. Assuming that this shortening strain can be extrapolated across the entire northern frontal range in the Qilian Shan, our analyses suggest that 50 km of north-south Cenozoic shortening has been accommodated along the northern margin of the Tibetan Plateau.

3. The internal regions of northern Tibet (i.e., the Qaidam Basin, North Qaidam, and Qilian Shan–Nan Shan thrust belts) and the northern plateau margin have absorbed >30%–45% and >53% Cenozoic shortening strain, respectively. To explain this strain distribution, we suggest that the dominant processes of plateau construction operating in northern Tibet are a combination of distributed crustal shortening, pure shear thickening, and southward underthrusting of the Asian mantle lithosphere. Most of the modern crustal thickness across the region can be explained by 30%–45% shortening of crust with an initial thickness of ~40 km. The higher strain recorded along the northern plateau margin may result from the southward underthrusting of Asian mantle lithosphere, which is supported by recent receiver function analysis (Ye et al., 2015). We present a 2-D lithospheric-scale model that relates these two deformation mechanisms to the observed strain in north Tibet.

4. We suggest that the 350-km-wide Qilian Shan–Nan Shan thrust belt has accommodated a minimum of 215–300 km of Cenozoic north-south shortening. Although detailed shortening estimates from the central Qilian Shan–Nan Shan thrust belt are lacking, we tentatively extrapolate the observed strain distribution to suggest that more than 250–350 km of north-south Cenozoic shortening has been absorbed within the Tibetan Plateau between the Kunlun fault in the south and the Hexi Corridor in the north, which is almost double the commonly cited shortening value of ~150 km.

5. Our analysis across the Qilian Shan frontal thrust system indicates that most of the present-day convergence between North China and Tibet is focused along the northern plateau margin, similar to Himalayan shortening where strain is concentrated along the Main Frontal Thrust (Lavé and Avouac, 2000; Burgess et al., 2012).

ACKNOWLEDGMENTS

This research was supported by grants from the Tectonics Program of the U.S. National Science Foundation (to Yin) and an East Asia and Pacific Summer Institutes summer fellowship funded jointly by the U.S. National Science Foundation and the China Science and Technology Exchange Center (to Zuza). We thank William Craddock and Delores Robinson for constructive reviews that improved the quality and clarity of this manuscript.

REFERENCES CITED

Allmendinger, R.W., Reilinger, R., and Loveless, J., 2007, Strain and rotation rate from GPS in Tibet, Anatolia, and the Altiplano: Tectonics, v. 26, TC3013, doi:10.1029/2006TC002030.

Ammon, C.J., Randall, G.E., and Zandt, G., 1990, On the nonuniqueness of receiver function inversions: Journal of Geophysical Research, v. 95, p. 15,303–15,318, doi:10.1029/JB095iB10p15303.

Argand, E., 1924, La Tectonique de l'Asie: Proceedings of the 13th International Geological Congress, v. 7, p. 171–372.

Bird, P., 1991, Lateral extrusion of lower crust from under high topography in the isostatic limit: Journal of Geophysical Research, v. 96, p. 10,275–10,286, doi:10.1029/91JB00370.

Bovet, P.M., Ritts, B.D., Gehrels, G., Abbink, A.O., Darby, B., and Hourigan, J., 2009, Evidence of Miocene crustal shortening in the north Qilian Shan from Cenozoic stratigraphy of the western Hexi Corridor, Gansu Province, China: American Journal of Science, v. 309, p. 290–329, doi:10.2475/00.4009.02.

Boyer, S.E., and Elliott, D., 1982, Thrust systems: American Association of Petroleum Geologists Bulletin, v. 66, p. 1196–1230.

Brown, L.D., Zhao, Wenjin, Nelson, K.D., Hauck, M., Alsdorf, D., Ross, A., Cogan, M., Clark, M., Liu, Xianwen, and Cheet, Jinkai, 1996, Bright spots, structure and magmatism in southern Tibet from INDEPTH seismic reflection profiling: Science, v. 274, p. 1688–1690, doi:10.1126/science.274.5293.1688.

Burchfiel, B.C., et al., 1991, Geology of the Haiyuan fault zone, Ningxia-Hui Autonomous Region, China, and its relation to the evolution of the northeastern margin of the Tibetan Plateau: Tectonics, v. 10, no. 6, p. 1091–1110.

Burchfiel, B.C., Zhiliang, C., Yupinc, L., and Royden, L.H., 1995, Tectonics of the Longmen Shan and adjacent regions, central China: International Geology Review, v. 37, p. 661–735, doi:10.1080/00206819509465424.

Burgess, W. P., Yin, A., Dubey, C. S., Shen, Z. K., and Kelty, T. K., 2012, Holocene shortening across the Main Frontal Thrust zone in the eastern Himalaya: Earth and Planetary Science Letters, v. 357, p. 152–167.

Geosphere, published online on 5 February 2016 as doi:10.1130/GES01254.1

Champagnac, J.D., Yuan, D.Y., Ge, W.P., Molnar, P., and Zheng, W.J., 2010, Slip rate at the north-eastern front of the Qilian Shan, China: Terra Nova, v. 22, p. 180–187, doi:10.1111/j.1365-3121.2010.00932.x.

Chen, J.H., Liu, Q.Y., Li, S.C., Guo, B., and Lai, Y.G., 2005, Crust and upper mantle S-wave velocity structure across northeastern Tibetan Plateau and Ordos block: Chinese Journal of Geophysics, v. 48, p. 369–379, doi:10.1002/cjg2.663.

Chen, Q.L., and Yang, Z.L., 2010, Petroleum geology of Pan-Hexi Corridor basins and exploration prospecting: Natural Gas Geoscience, v. 21, p. 186–192.

Chen, X., Yin, A., Gehrels, G.E., Cowgill, E.S., Grove, M., Harrison, T.M., and Wang, X.-F., 2003, Two phases of Mesozoic north-south extension in the eastern Altyn Tagh range, northern Tibetan Plateau: Tectonics, v. 22, 1053, doi:10.1029/2001TC001336.

Christensen, N., and Mooney, W., 1995, Seismic velocity structure and composition of the continental crust: A global view: Journal of Geophysical Research Atmospheres, v. 100, p. 761–9788.

Clark, M.K., and Royden, L.H., 2000, Topographic ooze: Building the eastern margin of Tibet by lower crustal flow: Geology, v. 28, p. 703–706, doi:10.1130/0091-7613(2000)28<703:TOBTEM>2.0.CO;2.

Clark, M. K., Schoenbohm, L. M., Royden, L. H., Whipple, K. X., Burchfiel, B. C., Zhang, X., Tang, W., Wang, E., and Chen, L., 2004, Surface uplift, tectonics, and erosion of eastern Tibet from large-scale drainage patterns: Tectonics, v. 23, doi:10.1029/2002TC00140.

Clark, M.K., Farley, K.A., Zheng, D., Wang, Z., and Duvall, A.R., 2010, Early Cenozoic faulting of the northern Tibetan Plateau margin from apatite (U-Th)/He ages: Earth and Planetary Science Letters, v. 296, p. 78–88, doi:10.1016/j.epsl.2010.04.051.

Cowgill, E., Yin, A., Harrison, T.M., and Wang, X.F., 2003, Reconstruction of the Altyn Tagh fault based on U-Pb geochronology: the role of backthrusts, mantle sutures, and heterogeneous crustal strength in forming the Tibetan plateau: Journal of Geophysical Research, v. 108, 2346, doi:10.1029/2002JB002080.

Craddock, W., Kirby, E., and Zhang, H., 2011, Late Miocene–Pliocene range growth in the interior of the northeastern Tibetan Plateau: Lithosphere, v. 3, p. 420–438, doi:10.1130/L159.1.

Craddock, W.H., Kirby, E., Zhang, H., Clark, M.K., Champagnac, J.D., and Yuan, D., 2014, Rates and style of Cenozoic deformation around the Gonghe Basin, northeastern Tibetan Plateau: Geosphere, v. 10, p. 1255–1282, doi:10.1130/GES01024.1.

Dahlstrom, C.D.A., 1969, Balanced cross section: Canadian Journal of Earth Sciences, v. 6, p. 743–757, doi:10.1139/e69-069.

Dang, J., 2011, Geochemical characteristics and tectonic implications of Jinfosi granite in north Qilian: Gansu Geology, v. 20, p. 40–44.

Dayem, K.E., Molnar, P., Clark, M.K., and Houseman, G.A., 2009, Far-field lithospheric deformation in Tibet during continental collision: Tectonics, v. 28, TC6005, doi:10.1029/2008TC002344.

DeCelles, P.G., Robinson, D.M., and Zandt, G., 2002, Implications of shortening in the Himalayan fold-thrust belt for uplift of the Tibetan Plateau: Tectonics, v. 21, 1062, doi:10.1029/2001TC001322.

Dewey, J.F., and Bird, J.M., 1970, Mountain belts and the new global tectonics: Journal of Geophysical Research, v. 75, p. 2625–2647, doi:10.1029/JB075i014p02625.

Dewey, J.F., and Burke, K.C., 1973, Tibetan, Variscan, and Precambrian basement reactivation: products of continental collision: Journal of Geology, v. 81, p. 683–692, doi:10.1086/627920.

Dewey, J. F., Cande, S., and Pitman, W. C., 1989, Tectonic evolution of the India/Eurasia collision zone: Eclogae Geologicae Helvetiae, v. 82, no. 3, p. 717–734.

Dupont-Nivet, G., Horton, B.K., Butler, R.F., Wang, J., Zhou, J., and Waanders, G.L., 2004, Paleogene clockwise tectonic rotation of the Xining-Lanzhou region, northeastern Tibetan Plateau: Journal of Geophysical Research, v. 109, no. B4, doi:10.1029/2003JB002620.

Duvall, A.R., Clark, M.K., van der Pluijm, B.A., and Li, C., 2011, Direct dating of Eocene reverse faulting in northeastern Tibet using Ar-dating of fault clays and low-temperature thermochronometry: Earth and Planetary Science Letters, v. 304, p. 520–526, doi:10.1016/j.epsl.2011.02.028.

Duvall, A.R., Clark, M.K., Kirby, E., Farley, K.A., Craddock, W.H., Li, C., and Yuan, D.Y., 2013, Low-temperature thermochronometry along the Kunlun and Haiyuan Faults, NE Tibetan Plateau: Evidence for kinematic change during late-stage orogenesis: Tectonics, v. 32, p. 1190–1211, doi:10.1002/tect.20072.

England, P., and Houseman, G., 1986, Finite strain calculations of continental deformation: 2. Comparison with the India-Asia collision zone: Journal of Geophysical Research, v. 91, no. B3, p. 3664–3676, doi:10.1029/JB091iB03p03664.

Fang, X., Zhao, Z., Li, J., Yan, M., Pan, B., Song, C., and Dai, S., 2004, Late Cenozoic magnetostratigraphy of Laojunmiao anticlines of northern Qilian shan (Mts.) and its implications for uplift of northern Tibetan Plateau: Science in China, v. 34, no. 2, p. 97–106.

Feng, M., Kumar, P., Mechie, J., Zhao, W., Kind, R., Su, H., Xue, G., Shi, D., and Qian, H., 2014, Structure of the crust and mantle down to 700 km depth beneath the East Qaidam basin and Qilian Shan from P and S receiver functions: Geophysical Journal International, v. 199, p. 1416–1429, doi:10.1093/gji/ggu335.

Fielding, E., Isacks, B., Barazangi, M., and Duncan, C., 1994, How flat is Tibet?: Geology, v. 22, p. 163–167, doi:10.1130/0091-7613(1994)022<0163:HFIT>2.3.CO;2.

Frederiksen, A.W., Folsom, H., and Zandt, G., 2003, Neighbourhood inversion of teleseismic Ps conversions for anisotropy and layer dip: Geophysical Journal International, v. 155, p. 200–212, doi:10.1046/j.1365-246X.2003.02043.x.

Gansu Geological Bureau, 1989, Regional geology of Gansu Province: Beijing, Geological Publishing House, 692 p. (in Chinese).

Gao, R., Cheng, X., and Wu, G., 1999, Lithospheric structure and geodynamic model of the Golmud–Ejn transect in northern Tibet, *in* Macfarlane, A., et al., eds., Himalaya and Tibet: Mountain roots to mountain tops: Geological Society of America Special Paper 328, p. 9–17, doi:10.1130/0-8137-2328-0.9.

Gao, R., Wang, H., Yin, A., Dong, S., Kuang, Z., Zuza, A.V., Li, W., and Xiong, X., 2013, Tectonic development of the northeastern Tibetan Plateau as constrained by high-resolution deep seismic-reflection data: Lithosphere, v. 5, p. 555–574, doi:10.1130/L293.1.

Gaudemer, Y., Tapponnier, P., Meyer, B., Peltzer, G., Shunmin, G., Zhitai, C., Huagung, D., and Cifuentes, I., 1995, Partitioning of crustal slip between linked, active faults in the eastern Qilian Shan, and evidence for a major seismic gap, the 'Tianzhu gap,' on the western Haiyuan fault, Gansu (China): Geophysical Journal International, v. 120, p. 599–645, doi:10.1111/j.1365-246X.1995.tb01842.x.

Gehrels, G.E., Yin, A., and Wang, X.F., 2003a, Detrital zircon geochronology of the northeastern Tibet: Geological Society of America Bulletin, v. 115, p. 881–896, doi:10.1130/0016-7606(2003)115<0881:DGOTNT>2.0.CO;2.

Gehrels, G.E., Yin, A., and Wang, X.F., 2003b, Magmatic history of the Altyn Tagh, Nan Shan, and Qilian Shan region of western China: Journal of Geophysical Research, v. 108, 2423, doi:10.1029/2002JB001876.

Godard, V., Pik, R., Lavé, J., Cattin, R., Tibari, B., De Sigoyer, J., Pubellier, M., and Zhu, J., 2009, Late Cenozoic evolution of the central Longmen Shan, eastern Tibet: Insight from (U-Th)/He thermochronometry: Tectonics, v. 28, TC5009, doi:10.1029/2008TC002407.

Groshong, R.H., Withjack, M.O., Schlische, R.W., and Hidayah, T.N., 2012, Bed length does not remain constant during deformation: recognition and why it matters: Journal of Structural Geology, v. 41, p. 86–97, doi:10.1016/j.jsg.2012.02.009.

He, G., and Pang, K., 2013, Seismic constraints on central Asian evolution of late Cenozoic: uplift rates and two-stage evolution of the northern Tibetan Plateau: China Journal of Earth Science and Climate Change, v. 4, no. 5, 4 p., doi:10.4172/2157-7617.1000152.

He, S., Wang, H., Xu, X., Zhang, H., and Ren, G., 2007, A LA-ICP-MS U-Pb chronological study of zircons from Hongtubu basic volcanic rocks and its geological significance in the east segment of North Qilian orogenic belt: Advances in Earth Science, v. 22, p. 143–151.

Hetzel, R., Tao, M., Stokes, S., Niedermann, S., Ivy-Ochs, S., Gao, B., Stecker, M.R., and Kubik, P.W., 2004, Late Pleistocene/Holocene slip rate of the Zhangye thrust (Qilian Shan, China) and implications for the active growth of the northeastern Tibetan Plateau: Tectonics, v. 23, TC6006, doi:10.1029/2004TC001653.

Horton, B.K., Yin, A., Spurlin, M.S., Zhou, J., and Wang, J., 2002, Paleocene–Eocene syncontractional sedimentation in narrow, lacustrine-dominated basins of east-central Tibet: Geological Society of America Bulletin, v. 114, p. 771–786, doi:10.1130/0016-7606(2002)114<0771:PESSIN>2.0.CO;2.

Horton, B.K., Dupont-Nivet, G., Zhou, J., Waanders, G.L., Butler, R.F., and Wang, J., 2004, Mesozoic–Cenozoic evolution of the Xining-Minhe and Dangchang basins, northeastern Tibetan Plateau: Magnetostratigraphic and biostratigraphic results: Journal of Geophysical Research, v. 109, no. B4, doi:10.1029/2003JB002913.

Hu, N.G., Xu, A.D., and Yang, J.X., 2005, Characteristics and tectonic environment of Zhigoumen pluton in Longshoushan area: Journal of Earth Sciences and Environment, v. 27, p. 5–11 (in Chinese with English abstract).

Hubbard, J., and Shaw, J.H., 2009, Uplift of the Longmen Shan and Tibetan plateau, and the 2008 Wenchuan (M= 7.9) earthquake: Nature, v. 458, no. 7235, p. 194–197, doi:10.1038/nature07837.

Geosphere, published online on 5 February 2016 as doi:10.1130/GES01254.1

Huo, Y.L., and Tan, S.D., 1995, Exploration case history and petroleum geology in Jiuquan continental basin: Beijing, China, Petroleum Industry Press, 211 p.

Johnson, M.R.W., 2002, Shortening budgets and the role of continental subduction during the India–Asia collision: Earth-Science Reviews, v. 59, p. 101–123, doi:10.1016/S0012-8252(02)00071-5.

Jolivet, M., Brunel, M., Seward, D., Xu, Z., Yang, J., Roger, F., Tapponnier, P., Malavieille, J., Arnaud, N., and Wu, C., 2001, Mesozoic and Cenozoic tectonics of the northern edge of the Tibetan plateau: Fission-track constraints: Tectonophysics, v. 343, p. 111–134, doi:10.1016/S0040-1951(01)00196-2.

Jolivet, M., Brunel, M., Seward, D., Xu, Z., Yang, J., Malavieille, J., Roger, F., Leyreloup, A., Arnaud, N., and Wu, C., 2003, Neogene extension and volcanism in the Kunlun fault zone, northern Tibet: New constraints on the age of the Kunlun Fault: Tectonics, v. 22, 1052, doi:10.1029/2002TC001428.

Kind, R., et al., 2002, Seismic images of crust and upper mantle beneath Tibet: Evidence for Eurasian plate subduction: Science, v. 298, no. 5596, p. 1219–1221, doi:10.1126/science.1078115.

King, R.W., Shen, F., Burchfiel, B.C., Royden, L.H., Wang, E., Chen, Z., Liu, Y., Zhang, X.-Y., Zhao, J.-X., and Li, Y., 1997, Geodetic measurement of crustal motion in southwest China: Geology, v. 25, p. 179–182, doi:10.1130/0091-7613(1997)025<0179:GMOCMI>2.3.CO;2.

Lavé, J., and Avouac, J. P., 2000, Active folding of fluvial terraces across the Siwaliks Hills, Himalayas of central Nepal: Journal of Geophysical Research, v. 105, no. B3, p. 5735–5770.

Lease, R.O., Burbank, D.W., Clark, M.K., Farley, K.A., Zheng, D., and Zhang, H., 2011, Middle Miocene reorganization of deformation along the northeastern Tibetan Plateau: Geology, v. 39, p. 359–362, doi:10.1130/G31356.1.

Lease, R.O., Burbank, D.W., Zhang, H., Liu, J., and Yuan, D., 2012, Cenozoic shortening budget for the northeastern edge of the Tibetan Plateau: Is lower crustal flow necessary?: Tectonics, v. 31, TC3011, doi:10.1029/2011TC003066.

Le Pichon, X., Fournier, M., and Jolivet, L., 1992, Kinematics, topography, shortening, and extrusion in the India-Eurasia collision: Tectonics, v. 11, p. 1085–1098, doi:10.1029/92TC01566.

Li, Y.L., 1993, Uplift of the Qinghai-Xizang Plateau and the affect to environment, *in* Bao, H.S., ed., Proceedings of geography research: Nanjing, Nanjing University Publishing House, p. 41–52 (in Chinese).

Li, Y.L., 1994, Mechanism and evolution of tectonic landforms in Hexi Corridor, Gansu [PhD thesis]: Peking University (in Chinese).

Li, Y.L., and Yang, J.C., 1998, Tectonic geomorphology in the Hexi Corridor, north-west China: Basin Research, v. 10, p. 345–352, doi:10.1046/j.1365-2117.1998.00070.x.

Lin, Y.H., Zhang, L.F., Ji, J.Q., and Song, S.G., 2010, $^{40}Ar/^{39}Ar$ age of Jiugequan lawsonite blueschists in northern Qilian Mountains and its petrologic significance: Chinese Science Bulletin, v. 55, p. 2021–2027, doi:10.1007/s11434-010-3239-8.

Liu, M., Mooney, W.D., Li, S., Okaya, N., and Detweiler, S., 2006, Crustal structure of the northeastern margin of the Tibetan plateau from the Songpan-Ganzi terrane to the Ordos basin: Tectonophysics, v. 420, p. 253–266, doi:10.1016/j.tecto.2006.01.025.

Liu, Y. J., Neubauer, F., Genser, J., Takasu, A., Ge, X. H., and Handler, R., 2006, $^{40}Ar/^{39}Ar$ ages of blueschist facies pelitic schists from Qingshuigou in the Northern Qilian Mountains, western China: Island Arc, v. 15, no. 1, p. 187–198.

Long, S., McQuarrie, N., Tobgay, T., and Grujic, D., 2011, Geometry and crustal shortening of the Himalayan fold-thrust belt, eastern and central Bhutan: Geological Society of America Bulletin, v. 123, p. 1427–1447, doi:10.1130/B30203.1.

Makovsky, Y., and Klemperer, S.L., 1999, Measuring the seismic properties of Tibetan bright spots: Evidence for free aqueous fluids in the Tibetan middle crust: Journal of Geophysical Research, v. 104, p. 10,795–10,825, doi:10.1029/1998JB900074.

McQuarrie, N., Robinson, D., Long, S., Tobgay, T., Grujic, D., Gehrels, G., and Ducea, M., 2008, Preliminary stratigraphic and structural architecture of Bhutan: Implications for the along strike architecture of the Himalayan system: Earth and Planetary Science Letters, v. 272, p. 105–117, doi:10.1016/j.epsl.2008.04.030.

Meyer, B., Tapponnier, P., Bourjot, L., Métivier, F., Gaudemer, Y., Peltzer, G., Shunmin, G., and Zhitai, C., 1998, Crustal thickening in Gansu-Qinghai, lithospheric mantle subduction, and oblique, strike-slip controlled growth of the Tibet Plateau: Geophysical Journal International, v. 135, p. 1–47, doi:10.1046/j.1365-246X.1998.00567.x.

Mock, C., Arnaud, N.O., and Cantagrel, J.M., 1999, An early unroofing in northeastern Tibet? Constraints from $^{40}Ar/^{39}Ar$ thermochronology on granitoids from the eastern Kunlun range (Qianghai, NW China): Earth and Planetary Science Letters, v. 171, p. 107–122, doi:10.1016/S0012-821X(99)00133-8.

Molnar, P., 1988, Continental tectonics in the aftermath of plate tectonics: Nature, v. 335, no. 6186, p. 131–137, doi:10.1038/335131a0.

Molnar, P., and Tapponnier, P., 1975, Cenozoic tectonics of Asia: Effects of a continental collision: Science, v. 189, no. 4201, p. 419–426, doi:10.1126/science.189.4201.419.

Molnar, P., England, P., and Martinod, J., 1993, Mantle dynamics, uplift of the Tibetan Plateau, and the Indian monsoon: Reviews of Geophysics, v. 31, p. 357–396, doi:10.1029/93RG02030.

Murphy, M.A., Yin, A., Harrison, T.M., Dürr, S.B., Chen, Z., Ryerson, F.J., Kidd, S.F., Wang, X., and Zhou, X., 1997, Did the Indo-Asian collision alone create the Tibetan plateau?: Geology, v. 25, p. 719–722, doi:10.1130/0091-7613(1997)025<0719:DTIACA>2.3.CO;2.

Pan, G., Ding, J., Yao, D., and Wang, L., 2004, Geological map of Qinghai-Xiang (Tibet) plateau and adjacent areas: Chengdu, China, Chengdu Institute of Geology and Mineral Resources, China Geological Survey, Chengdu Cartographic Publishing House, scale 1:1,500,000.

Pan, S., and Niu, F., 2011, Large contrasts in crustal structure and composition between the Ordos plateau and the NE Tibetan plateau from receiver function analysis: Earth and Planetary Science Letters, v. 303, p. 291–298, doi:10.1016/j.epsl.2011.01.007.

Powell, C.M., 1986, Continental underplating model for the rise of the Tibetan Plateau: Earth and Planetary Science Letters, v. 81, p. 79–94, doi:10.1016/0012-821X(86)90102-0.

Powell, C.M.A., and Conaghan, P.J., 1973, Polyphase deformation in Phanerozoic rocks of the Central Himalayan Gneiss, northwest India: Journal of Geology, v. 81, p. 127–143, doi:10.1086/627830.

Pullen, A., Kapp, P., Gehrels, G.E., Vervoort, J.D., and Ding, L., 2008, Triassic continental subduction in central Tibet and Mediterranean-style closure of the Paleo-Tethys Ocean: Geology, v. 36, p. 351–354, doi:10.1130/G24435A.1.

Qian, Q., Wang, Y.M., Li, H.M., Jia, X.Q., Han, S., and Zhang, Q., 1998, Geochemical characteristics and genesis of diorites from Laohushan, Gansu Province: Acta Petrolei Sinica, v. 14, p. 520–528 (in Chinese with English abstract).

Qinghai BGMR (Bureau of Geology and Mineral Resources), 1991, Regional geology of Qinghai Province: Beijing, China, Geological Publishing House, 662 p.

Quan, S., Jia, Q., Guo, Z., and Wang, W., 2006, Basic characteristics of granitoids related to tungsten mineralization in the Qilian mountain: Mineralium Deposita, v. 25, p. 143–146.

Reith, R.C., 2013, Structural geology of a central segment of the Qilian Shan-Nan Shan thrust belt: Implications for the magnitude of Cenozoic shortening in the northeastern Tibetan Plateau [M.S. thesis]: Los Angeles, University of California, 73 p.

Robinson, D.M., DeCelles, P.G., and Copeland, P., 2006, Tectonic evolution of the Himalayan thrust belt in western Nepal: Implications for channel flow models: Geological Society of America Bulletin, v. 118, p. 865–885, doi:10.1130/B25911.1.

Rohrmann, A., Kapp, P., Carrapa, B., Reiners, P.W., Guynn, J., Ding, L., and Heizler, M., 2012, Thermochronologic evidence for plateau formation in central Tibet by 45 Ma: Geology, v. 40, p. 187–190, doi:10.1130/G32530.1.

Royden, L.H., Burchfiel, B.C., King, R.W., Wang, E., Chen, Z., Shen, F., and Liu, Y., 1997, Surface deformation and lower crustal flow in eastern Tibet: Science, v. 276, no. 5313, p. 788–790, doi:10.1126/science.276.5313.788.

Royden, L.H., Burchfiel, B.C., and van der Hilst, R.D., 2008, The geological evolution of the Tibetan Plateau: Science, v. 321, no. 5892, p. 1054–1058, doi:10.1126/science.1155371.

Ryan, W.B.F., et al., 2009, Global multi-resolution topography synthesis: Geochemistry, Geophysics, Geosystems, v. 10, Q03014, doi:10.1029/2008GC002332.

Schubert, G., and Sandwell, D., 1989, Crustal volumes of the continents and of oceanic and continental submarine plateaus: Earth and Planetary Science Letters, v. 92, p. 234–246, doi:10.1016/0012-821X(89)90049-6.

Şengör, A.M.C., and Natal'in, B.A., 1996, Paleotectonics of Asia: Fragments of a synthesis, *in* Yin, A., and Harrison, T.M., eds., The tectonics of Asia: New York, Cambridge University Press, p. 486–640.

Sherrington, H.F., Zandt, G., and Frederiksen, A., 2004, Crustal fabric in the Tibetan plateau based on waveform inversions for seismic anisotropy parameters: Journal of Geophysical Research, v. 109, B02312, doi:10.1029/2002JB002345.

Smith, A.D., 2006, The geochemistry and age of ophiolitic strata of the Xinglongshan Group: Implications for the amalgamation of the Central Qilian belt: Journal of Asian Earth Sciences, v. 28, p. 133–142, doi:10.1016/j.jseaes.2005.09.014.

Sobel, E.R., and Arnaud, N., 1999, A possible middle Paleozoic suture in the Altyn Tagh, NW China: Tectonics, v. 18, p. 64–74, doi:10.1029/1998TC900023.

Song, S., Zhang, L.F., Niu, Y.L., Su, L., Song, B., and Liu, D.Y., 2006, Evolution from oceanic subduction to continental collision: A case study of the Northern Tibetan Plateau inferred from

Geosphere, published online on 5 February 2016 as doi:10.1130/GES01254.1

geochemical and geochronological data: Journal of Petrology, v. 47, p. 435–455, doi:10.1093/petrology/egi080.

Song, S., Niu, Y., Su, L., and Xia, X., 2013, Tectonics of the North Qilian orogen, NW China: Gondwana Research, v. 23, p. 1378–1401, doi:10.1016/j.gr.2012.02.004.

Su, J., Zhang, X., Hu, N., Fu, G., and Zhang, H., 2004, Geochemical characteristics and genesis of adakite-like granites at Yema Nanshan in the western segment of the Central Qilian Mountains: Chinese Geology, v. 31, p. 365–371.

Tapponnier, P., et al., 1990, Active thrusting and folding in the Qilian Shan, and decoupling between upper crust and mantle in northeastern Tibet: Earth and Planetary Science Letters, v. 97, p. 382–403, doi:10.1016/0012-821X(90)90053-Z.

Tapponnier, P., Zhiqin, X., Roger, F., Meyer, B., Arnaud, N., Wittlinger, G., and Jingsui, Y., 2001, Oblique stepwise rise and growth of the Tibet Plateau: Science, v. 294, no. 5547, p. 1671–1677, doi:10.1126/science.105978.

Taylor, M., and Yin, A., 2009, Active structures of the Himalayan-Tibetan orogen and their relationships to earthquake distribution, contemporary strain field, and Cenozoic volcanism: Geosphere, v. 5, p. 199–214, doi:10.1130/GES00217.1.

Tseng, C.Y., Yang, H.J., Yang, H.Y., Liu, D.Y., Tsai, C.L., Wu, H.Q., and Zuo, G.C., 2007, The Dongcaohe ophiolite from the North Qilian Mountains: A fossil oceanic crust of the paleo-Qilian ocean: Chinese Science Bulletin, v. 52, p. 2390–2401, doi:10.1007/s11434-007-0300-3.

Tseng, C.Y., Yang, H.J., Yang, H.Y., Liu, D., Wu, C., Cheng, C.K., Chen, C.H., and Ker, C.M., 2009, Continuity of the North Qilian and North Qinling orogenic belts, central orogenic system of China: Evidence from newly discovered Paleozoic adakitic rocks: Gondwana Research, v. 16, p. 285–293, doi:10.1016/j.gr.2009.04.003.

van Hinsbergen, D.J., Kapp, P., Dupont-Nivet, G., Lippert, P.C., DeCelles, P.G., and Torsvik, T.H., 2011, Restoration of Cenozoic deformation in Asia and the size of Greater India: Tectonics, v. 30, TC5003, doi:10.1029/2011TC002908.

van Hinsbergen, D.J., Lippert, P.C., Dupont-Nivet, G., McQuarrie, N., Doubrovine, P.V., Spakman, W., and Torsvik, T.H., 2012, Greater India Basin hypothesis and a two-stage Cenozoic collision between India and Asia: National Academy of Sciences Proceedings, v. 109, p. 7659–7664, doi:10.1073/pnas.1117262109.

Vergne, J., Wittlinger, G., Qiang, H., Tapponnier, P., Poupinet, G., Jiang, M., Herquel, G., and Paul, A., 2002, Seismic evidence for stepwise thickening of the crust across the NE Tibetan Plateau: Earth and Planetary Science Letters, v. 203, p. 25–33, doi:10.1016/S0012-821X(02)00853-1.

Vergne, J., Wittlinger, G., Farra, V., and Su, H., 2003, Evidence for upper crustal anisotropy in the Songpan-Ganze (northeastern Tibet) terrane: Geophysical Research Letters, v. 30, 1552, doi:10.1029/2002GL016847.

Vincent, S.J., and Allen, M.B., 1999, Evolution of the Minle and Chaoshui Basins, China: Implications for Mesozoic strike-slip basin formation in Central Asia: Geological Society of America Bulletin, v. 111, p. 725–742, doi:10.1130/0016-7606(1999)111<0725:EOTMAC>2.3.CO;2.

Wallis, S., Tsujimori, T., Aoya, M., Kawakami, T., Terada, K., Suzuki, K., and Hyodo, H., 2003, Cenozoic and Mesozoic metamorphism in the Longmenshan orogen: Implications for geodynamic models of eastern Tibet: Geology, v. 31, p. 745–748, doi:10.1130/G19562.1.

Wang, C., Zhao, X., Liu, Z., Lippert, P.C., Graham, S.A., Coe, R.S., Yi, H., Zhu, L., Liu, S., and Li, Y.-l., 2008, Constraints on the early uplift history of the Tibetan Plateau: National Academy of Sciences Proceedings, v. 105, p. 4987–4992, doi:10.1073/pnas.0703595105.

Wang, C., Gao, R., Yin, A., Wang, H., Zhang, Y., Guo, T., Li, Q., and Li, Y., 2011, A mid-crustal strain-transfer model for continental deformation: A new perspective from high-resolution deep seismic-reflection profiling across NE Tibet: Earth and Planetary Science Letters, v. 306, p. 279–288, doi:10.1016/j.epsl.2011.04.010.

Wang, Q.M., and Coward, M.P., 1993, The Jiuxi basin, Hexi corridor, NW China: Foreland structural features and hydrocarbon potential: Journal of Petroleum Geology, v. 16, p. 169–182, doi:10.1111/j.1747-5457.1993.tb00104.x.

Webb, A.A.G., 2013, Preliminary balanced palinspastic reconstruction of Cenozoic deformation across the Himachal Himalaya (northwestern India): Geosphere, v. 9, p. 572–587, doi:10.1130/GES00787.1.

Webb, A.A.G., Yin, A., Harrison, T.M., Célérier, J., Gehrels, G.E., Manning, C.E., and Grove, M., 2011, Cenozoic tectonic history of the Himachal Himalaya (northwestern India) and its constraints on the formation mechanism of the Himalayan orogen: Geosphere, v. 7, p. 1013–1061, doi:10.1130/GES00627.1.

Willett, S.D., and Beaumont, C., 1994, Subduction of Asian lithospheric mantle beneath Tibet inferred from models of continental collision: Nature, v. 369, no. 6482, p. 642–645, doi:10.1038/369642a0.

Worley, B.A., and Wilson, C.J., 1996, Deformation partitioning and foliation reactivation during transpressional orogenesis, an example from the Central Longmen Shan, China: Journal of Structural Geology, v. 18, p. 395–411, doi:10.1016/0191-8141(95)00095-U.

Wu, C.L., Yang, J.S., Yang, H.Y., Wooden, J., Shi, R.D., Chen, S.Y., and Zheng, Q.G., 2004, Dating of two types of granite from north Qilian, China: Acta Petrolei Sinica, v. 20, p. 425–432.

Wu, C.L., Yao, S., Zeng, L., Yang, J., Wooden, J., Chen, S., and Mazadab, F., 2006, Double subduction of the early Paleozoic North Qilian oceanic plate: Evidence from granites in the central segment of North Qilian, NW China: Geology in China, v. 33, p. 1197–1208.

Wu, C.L., Xu, X.Y., Gao, Q.M., Li, X.M., Lei, M., Gao, Y.H., Frost, B.R., and Wooden, J., 2010, Early Palaeozoic granitoid magmatism and tectonic evolution in North Qilian, NW China: Yanshi Xuebao, v. 26, p. 1027–1044 (in Chinese with English abstract).

Wu, J., Tang, Q.S., Chen, H.L., Xiao, A.C., Cheng, X.G., and Mao, Q.M., 2006, The thrust deformation of pluton: Take the Jinfosi pluton in eastern Jiuquan Basin as an example: Geological Journal of China Universities, v. 12, p. 22–29 (in Chinese with English abstract).

Xia, X.H., and Song, S.G., 2010, Forming age and tectono-petrogenesis of the Jiugequan ophiolite in the North Qilian Mountain, NW China: Chinese Science Bulletin, v. 55, p. 1899–1907, doi:10.1007/s11434-010-3207-3.

Xia, X.H., Song, S., and Niu, Y., 2012, Tholeiite-boninite terrane in the North Qilian suture zone: Implications for subduction initiation and back-arc basin development: Chemical Geology, v. 328, p. 259–277, doi:10.1016/j.chemgeo.2011.12.001.

Xiang, Z.Q., Lu, S.N., Li, H.K., Li, H.M., Song, B., and Zheng, J.K., 2007, SHRIMP U-Pb zircon age of gabbro in Aoyougou in the western segment of the North Qilian Mountains, China and its geological implications: Geological Bulletin of China, v. 26, p. 1686–1691.

Xiao, W., Windley, B.F., Yong, Y., Yan, Z., Yuan, C., Liu, C., and Li, J., 2009, Early Paleozoic to Devonian multiple-accretionary model for the Qilian Shan, NW China: Journal of Asian Earth Sciences, v. 35, p. 323–333, doi:10.1016/j.jseaes.2008.10.001.

Xiong, Z., Zhang, H., and Zhang, J., 2012, Petrogenesis and tectonic implications of the Maozangsi and Huangyanghe granitic intrusions in Lenglongling area, the eastern part of North Qilian Mountain, NW China: Earth Science Frontiers, v. 19, p. 214–227.

Yakovlev, P.V., and Clark, M.K., 2014, Conservation and redistribution of crust during the Indo-Asian collision: Tectonics, v. 33, p. 1016–1027, doi:10.1002/2013TC003469.

Yang, J.C., Zheng, W.T., and Li, Y.L., 1993, Evolution model of the compressive basins in the Hexi Corridor, *in* Bao, H.S., ed., Proceeding of geography research: Nanjing, China, Nanjing University Publishing House, p. 133–144 (in Chinese).

Yang, S., Cheng, X., Xiao, A., Chen, J., Fan, M., and Tain, D., 2007a, The structural characteristics of Northern Qilian Shan mountain thrust belt and its control on the oil and gas accumulation: Beijing, China, Science Press, p. 70–82 (in Chinese).

Yang, S., Chen, H., Cheng, X., Xiao, A., He, G., Chen, J., and Tian, D., 2007b, Deformation characteristics and rules of spatial change for the Northern Qilianshan thrust belt: Earth Science Frontiers, v. 14, p. 211–221.

Ye, Z., Gao, R., Li, Q., Zhang, H., Shen, X., Liu, X., and Gong, C., 2015, Seismic evidence for the North China plate underthrusting beneath northeastern Tibet and its implications for plateau growth: Earth and Planetary Science Letters, v. 426, p. 109–117, doi:10.1016/j.epsl.2015.06.024.

Yin, A., 2006, Cenozoic tectonic evolution of the Himalayan orogen as constrained by along-strike variation of structural geometry, exhumation history, and foreland sedimentation: Earth-Science Reviews, v. 76, p. 1–131, doi:10.1016/j.earscirev.2005.05.004.

Yin, A., 2010, Cenozoic tectonic evolution of Asia: A preliminary synthesis: Tectonophysics, v. 488, p. 293–325, doi:10.1016/j.tecto.2009.06.002.

Yin, A., and Harrison, T.M., 2000, Geologic evolution of the Himalayan-Tibetan orogen: Annual Review of Earth and Planetary Sciences, v. 28, p. 211–280, doi:10.1146/annurev.earth.28.1.211.

Yin, A., and Nie, S., 1993, An indentation model for the North and South China collision and the development of the Tan-Lu and Honam fault systems, eastern Asia: Tectonics, v. 12, no. 4, p. 801–813.

Yin, A., and Nie, S., 1996, A Phanerozoic palinspastic reconstruction of China and its neighboring regions, *in* Yin, A., and Harrison, T.M., eds., The tectonics of Asia: New York, Cambridge University Press, p. 442–485.

Yin, A., Dang, Y.-Q., Zhang, M., McRivette, M.W., Burgess, W.P., and Chen, X.-H., 2007a, Cenozoic tectonic evolution of Qaidam Basin and its surrounding regions (part 2): Wedge tectonics in southern Qaidam Basin and the Eastern Kunlun Range, *in* Sears, J.W., et al., eds., Whence the Mountains? Inquiries into the evolution of orogenic systems: A volume in honor of Raymond A. Price: Geological Society of America Special Paper 433, p. 369–390, doi:10.1130/2007.2433(18).

Geosphere, published online on 5 February 2016 as doi:10.1130/GES01254.1

Yin, A., Manning, C.E., Lovera, O., Menold, C.A., Chen, X., and Gehrels, G.E., 2007b, Early Paleozoic tectonic and thermomechanical evolution of ultrahigh-pressure (UHP) metamorphic rocks in the northern Tibetan Plateau, northwest China: International Geology Review, v. 49, p. 681–716, doi:10.2747/0020-6814.49.8.681.

Yin, A., Dang, Y.-Q., Wang, L.-C., Jiang, W.-M., Zhou, S.-P., Chen, X.-H., Gehrels, G.E., and McRivette, M.W., 2008a, Cenozoic tectonic evolution of Qaidam Basin and its surrounding regions (part 1): The southern Qilian Shan–Nan Shan thrust belt and northern Qaidam Basin: Geological Society of America Bulletin, v. 120, p. 813–846, doi:10.1130/B26180.1.

Yin, A., Dang, Y.Q., Zhang, M., Chen, X.H., and McRivette, M.W., 2008b, Cenozoic tectonic evolution of the Qaidam basin and its surrounding regions (Part 3): Structural geology, sedimentation, and regional tectonic reconstruction: Geological Society of America Bulletin, v. 120, p. 847–876, doi:10.1130/B26232.1.

Yin, A., Dubey, C.S., Webb, A.A.G., Kelty, T.K., Grove, M., Gehrels, G.E., and Burgess, W.P., 2010a, Geologic correlation of the Himalayan orogen and Indian craton: Part 1. Structural geology, U-Pb zircon geochronology, and tectonic evolution of the Shillong Plateau and its neighboring regions in NE India: Geological Society of America Bulletin, v. 122, p. 336–359, doi:10.1130/B26460.1.

Yin, A., Dubey, C.S., Kelty, T.K., Webb, A.A.G., Harrison, T.M., Chou, C.Y., and Célérier, J., 2010b, Geologic correlation of the Himalayan orogen and Indian craton: Part 2. Structural geology, geochronology, and tectonic evolution of the Eastern Himalaya: Geological Society of America Bulletin, v. 122, p. 360–395, doi:10.1130/B26461.1.

Yuan, D. Y., et al., 2011, Late Quaternary right-lateral slip rates of faults adjacent to the lake Qinghai, northeastern margin of the Tibetan Plateau: Geological Society of America Bulletin, v. 123, p. 2016–2030, doi:10.1130/B30315.1.

Yuan, D.Y., et al., 2013, The growth of northeastern Tibet and its relevance to large-scale continental geodynamics: A review of recent studies: Tectonics, v. 32, p. 1358–1370, doi:10.1002/tect.20081.

Yue, H., et al., 2012, Lithospheric and upper mantle structure of the northeastern Tibetan Plateau: Journal of Geophysical Research, v. 117, no. B5, B05307, doi:10.1029/2011JB008545.

Zhang, Z.H., 1990, Quaternary Geological Map of China and Adjacent Seas (1:2500000): Beijing, Cartographic Publishing House.

Zhang, D.Q., Sun, G.Y., and Xu, H.L., 1995, Petrology and isotope chronology of the Jinfosi pluton, Qilian Mts., Gansu: Acta Geoscientia Sinica, v. 37, p. 375–385 (in Chinese with English abstract).

Zhang, H.-P., Craddock, W.H., Lease, R.O., Wang, W.-T., Yuan, D.-Y., Zhang, P.-Z., Molnar, P., Zheng, D.-W., and Zheng, W.-J., 2012, Magnetostratigraphy of the Neogene Chaka Basin and its implications for mountain building processes in the north-eastern Tibetan Plateau: Basin Research, v. 24, p. 31–50, doi:10.1111/j.1365-2117.2011.00512.x.

Zhang, J.X., Meng, F.C., and Wan, Y.S., 2007, A cold early Palaeozoic subduction zone in the North Qilian Mountains, NW China: Petrological and U-Pb geochronological constraints: Journal of Metamorphic Geology, v. 25, p. 285–304, doi:10.1111/j.1525-1314.2006.00689.x.

Zhang, P.Z., et al., 2004, Continuous deformation of the Tibetan Plateau from global positioning system data: Geology, v. 32, p. 809–812, doi:10.1130/G20554.1.

Zhang, Z.M., Dong, X., Santosh, M., and Zhao, G.C., 2014, Metamorphism and tectonic evolution of the Lhasa terrane, Central Tibet: Gondwana Research, v. 25, p. 170–189, doi:10.1016/j.gr.2012.08.024.

Zhao, R., Zhao, Z., Fan, W., Zhou, Z., and Mao, J., 2002, Geology of Gansu Province: Bureau of Geology and mineral resources of Gansu Province, *in* Geological Atlas of China: Beijing, China, Geological Publishing House, p. 325–332.

Zhao, W., et al., 2001, Crustal structure of central Tibet as derived from project INDEPTH wide-angle seismic data: Geophysical Journal International, v. 145, p. 486–498, doi:10.1046/j.0956-540x.2001.01402.x.

Zhao, W., et al., 2011, Tibetan plate overriding the Asian plate in central and northern Tibet: Nature Geoscience, v. 4, p. 870–873, doi:10.1038/ngeo1309.

Zhao, W.-L., and Morgan, W.J., 1987, Injection of Indian crust into Tibetan lower crust: A two-dimensional finite element model study: Tectonics, v. 6, p. 489–504, doi:10.1029/TC006i004p00489.

Zheng, D., Zhang, P.Z., Wan, J., Yuan, D., Li, C., Yin, G., Zhang, G., Wang, Z., Min, W., and Chen, J., 2006, Rapid exhumation at ~8 Ma on the Liupan Shan thrust fault from apatite fission-track thermochronology: Implications for growth of the northeastern Tibetan Plateau margin: Earth and Planetary Science Letters, v. 248, p. 198–208, doi:10.1016/j.epsl.2006.05.023.

Zheng, D., Clark, M.K., Zhang, P., Zheng, W., and Farley, K.A., 2010, Erosion, fault initiation and topographic growth of the North Qilian Shan (northern Tibetan Plateau): Geosphere, v. 6, p. 937–941, doi:10.1130/GES00523.1.

Zheng, W.J., Zhang, P.Z., Yuan, D.Y., Zheng, D.W., Li, C., Zhang, P., Yin, J., Min, W., Heermance, R., and Chen, J., 2009, Deformation on the northern of the Tibetan Plateau from GPS measurement and geologic rates of the late Quaternary along the major fault: Chinese Journal of Geophysics, v. 52, p. 2491–2508.

Zheng, W.J., Zhang, P.Z., He, W.G., Yuan, D.Y., Shao, Y.X., Zheng, D.W., Ge, W.P., and Min, W., 2013, Transformation of displacement between strike-slip and crustal shortening in the northern margin of the Tibetan Plateau: Evidence from decadal GPS measurements and late Quaternary slip rates on faults: Tectonophysics, v. 584, p. 267–280, doi:10.1016/j.tecto.2012.01.006.

Zhiyi, Z., and Dean, W.T., 1996, Phanerozoic geology of northwest China: Beijing, China, Science Press, 316 p.

Zhou, J., Xu, F., Wang, T., Cao, A., and Yin, C., 2006, Cenozoic deformation history of the Qaidam Basin, NW China: Results from cross-section restoration and implications for Qinghai–Tibet Plateau tectonics: Earth and Planetary Science Letters, v. 243, p. 195–210, doi:10.1016/j.epsl.2005.11.033.

Zhu, B., Kidd, W.S., Rowley, D.B., Currie, B.S., and Shafique, N., 2005, Age of initiation of the India-Asia collision in the east-central Himalaya: Journal of Geology, v. 113, p. 265–285, doi:10.1086/428805.

Zhuang, G., Hourigan, J.K., Ritts, B.D., and Kent-Corson, M.L., 2011, Cenozoic multiple-phase tectonic evolution of the northern Tibetan Plateau: constraints from sedimentary records from Qaidam basin, Hexi Corridor, and Subei basin, northwest China: American Journal of Science, v. 311, no. 2, p. 116–152.

Geosphere, published online on 5 February 2016 as doi:10.1130/GES01254.1

Geosphere

Testing models of Tibetan Plateau formation with Cenozoic shortening estimates across the Qilian Shan–Nan Shan thrust belt

Andrew V. Zuza, Xiaogan Cheng and An Yin

Geosphere published online 5 February 2016;
doi: 10.1130/GES01254.1

Email alerting services click www.gsapubs.org/cgi/alerts to receive free e-mail alerts when new articles cite this article

Subscribe click www.gsapubs.org/subscriptions/ to subscribe to Geosphere

Permission request click http://www.geosociety.org/pubs/copyrt.htm#gsa to contact GSA

Copyright not claimed on content prepared wholly by U.S. government employees within scope of their employment. Individual scientists are hereby granted permission, without fees or further requests to GSA, to use a single figure, a single table, and/or a brief paragraph of text in subsequent works and to make unlimited copies of items in GSA's journals for noncommercial use in classrooms to further education and science. This file may not be posted to any Web site, but authors may post the abstracts only of their articles on their own or their organization's Web site providing the posting includes a reference to the article's full citation. GSA provides this and other forums for the presentation of diverse opinions and positions by scientists worldwide, regardless of their race, citizenship, gender, religion, or political viewpoint. Opinions presented in this publication do not reflect official positions of the Society.

Advance online articles have been peer reviewed and accepted for publication but have not yet appeared in the paper journal (edited, typeset versions may be posted when available prior to final publication). Advance online articles are citable and establish publication priority; they are indexed by GeoRef from initial publication. Citations to Advance online articles must include the digital object identifier (DOIs) and date of initial publication.

© Geological Society of America

THE
GEOLOGICAL
SOCIETY
OF AMERICA

Geosphere, published online on 5 February 2016 as doi:10.1130/GES01254.1

Notes

Advance online articles have been peer reviewed and accepted for publication but have not yet appeared in the paper journal (edited, typeset versions may be posted when available prior to final publication). Advance online articles are citable and establish publication priority; they are indexed by GeoRef from initial publication. Citations to Advance online articles must include the digital object identifier (DOIs) and date of initial publication.

© Geological Society of America

THE
GEOLOGICAL
SOCIETY
OF AMERICA